Indonesian Journal of Science & Technology

Journal homepage: http://ejournal.upi.edu/index.php/ijost/

A Multi-Analytical Study of Ultrasound-Assisted Extraction of *Annona muricata* Leaves with Bioactive Quality

Dessy Agustina Sari[1,2], Moh. Djaeni[1,], Setia Budi Sasongko[1], Ching Lik Hii[3], Aji Prasetyaningrum[1], Andri Cahyo Kumoro[1], Chung Lim Law[3]*

[1]Department of Chemical Engineering, Universitas Diponegoro, Semarang 50275, Indonesia
[2]Chemical Engineering Program, Universitas Singaperbangsa Karawang, Karawang 41361, Indonesia
[3]Department of Chemical and Environmental Engineering, University of Nottingham Malaysia, Selangor Darul Ehsan, Malaysia
*Correspondence: E-mail: moh.djaeni@live.undip.ac.id

ABSTRACT

This study compared ultrasonic-assisted extraction (UAE) with conventional Soxhlet extraction to evaluate the effect of solvent composition (ethanol–water 70:30–100:0), ultrasonic power rate (10–90%), and extraction time (2.5–15 min) on bioactive release and extraction kinetics. Extraction performance was assessed using a hierarchical framework consisting of extraction yield, total phenolic content normalized to yield (yield × TPC), and total flavonoid content normalized to yield (yield × TFC), followed by functional and chemical characterization through antioxidant activity (IC^{50}), phytochemical profiling, colorimetry, FTIR spectroscopy, GC–MS, and HPLC analysis. The results showed that solvent polarity, ultrasonic power rate, and extraction time significantly affected extraction efficiency ($p < 0.001$). Under optimal UAE conditions (70:30–85:15 ethanol–water, moderate ultrasonic power, and 5–7.5 min extraction), yields reached 3.6–4.1%, which equates to a 17–368% increase compared to Soxhlet extraction. Overall, UAE produced chemically richer, more stable, and more bioactive extracts than Soxhlet extraction, while significantly reducing extraction time, demonstrating its potential as a rapid and energy-efficient method for producing high-quality *A. muricata* leaf extracts for natural product applications.

ARTICLE INFO

Article History:
Submitted/Received 19 Dec 2025
First Revised 17 Mar 2026
Accepted 04 Apr 2026
First Available Online 29 Apr 2026
Publication Date 30 Apr 2026

Keyword:
Bioactive compound,
Kinetic model of extraction,
Quercetin,
Soursop leaves,
UAE.

1. INTRODUCTION

Natural products remain an important source of bioactive compounds for pharmaceuticals, nutraceuticals, and functional foods. Among medicinal plants, *Annona muricata* (soursop) has attracted considerable scientific attention because its leaves contain diverse phytochemicals, including phenolics, flavonoids, acetogenins, alkaloids, and saponins, which contribute to antioxidant, anti-inflammatory, antimicrobial, and anticancer activities [1,2]. Phenolic and flavonoid compounds are particularly important because they largely determine the antioxidant capacity and functional stability of plant extracts. Among these compounds, quercetin is frequently reported as a dominant flavonoid and is often used as a representative antioxidant marker in *A. muricata* leaves [3,4]. Consequently, efficient extraction strategies are required to maximize the recovery of these compounds while preserving their structural integrity.

Extraction efficiency from plant matrices is strongly influenced by the method and operating conditions employed. Conventional Soxhlet extraction is widely used because of its reproducibility; however, it typically requires long extraction times and prolonged heating, which may degrade thermolabile phytochemicals [2,5]. In contrast, ultrasound-assisted extraction (UAE) uses acoustic cavitation to enhance solvent penetration, disrupt plant cell walls, and accelerate mass transfer. Previous studies have reported that UAE can increase phenolic recovery by approximately 20–60% while reducing extraction time from several hours to only a few minutes, depending on the plant matrix [1,6,7]. UAE generally performs best when hydro-alcoholic solvents and moderate ultrasonic intensities are used because these conditions balance solvent polarity and cavitation energy [8,9]. Nevertheless, many studies evaluate extraction performance using only a single indicator, such as extraction yield or total phenolic content, which limits mechanistic interpretation of how ultrasonic parameters influence bioactive release.

Despite growing interest in medicinal plants in the UAE, several important knowledge gaps remain regarding *A. muricata* leaves. Most previous studies have focused on either extraction yield or antioxidant activity without simultaneously examining extraction kinetics, phenolic–flavonoid retention, and structural modifications of the plant matrix [4,10,11]. In addition, analytical characterization is often conducted using a single technique, which restricts the ability to link extraction conditions with molecular-level structural changes and the resulting bioactive composition. As a consequence, the mechanistic relationship between ultrasonic cavitation, plant-matrix disruption, and bioactive compound release remains insufficiently understood. A systematic analytical framework that integrates extraction efficiency indicators with complementary spectroscopic and chromatographic techniques is therefore required to better interpret how ultrasound modifies plant matrices and influences phytochemical recovery.

To address these limitations, the present study adopts a hierarchical multi-indicator evaluation framework combined with integrated analytical characterization. Extraction efficiency was first evaluated using primary indicators (yield, yield-normalized total phenolic content (yield × TPC), and yield-normalized total flavonoid content (yield × TFC)) that quantify the recovery of major antioxidant compounds. These indicators were subsequently linked to functional quality parameters, including antioxidant activity (IC_{50}), phytochemical groups (tannins, alkaloids, saponins, and steroids), and color stability indices (L, a*, b*), which reflect chemical degradation during extraction [2,12]. Structural and molecular characterization was then performed using FTIR spectroscopy to assess plant-matrix disruption, GC–MS to identify volatile and semi-volatile compounds, and HPLC to quantify quercetin, a representative

DOI: https://doi.org/10.17509/ijost.v11i1.94654
p- ISSN 2528-1410 e- ISSN 2527-8045

flavonoid marker. The integration of these analytical techniques enables the relationship between cavitation-induced structural changes, phytochemical composition, and antioxidant functionality to be interpreted within a single experimental framework.

Based on this integrated framework, this study aims to: (i) quantitatively compare ultrasound-assisted extraction and Soxhlet extraction for *A. muricata* leaves using hierarchical extraction indicators (yield, yield × TPC, and yield × TFC); (ii) evaluate the influence of solvent ratio, ultrasonic power rate, and extraction time on extraction kinetics and bioactive retention; and (iii) integrate multi-analytical characterization—including antioxidant assays, phytochemical analysis, color measurement, FTIR spectroscopy, GC–MS profiling, and HPLC quantification—to elucidate the relationship between cavitation-induced structural changes and bioactive compound release. By combining kinetic modeling with multi-analytical characterization, this study provides a more comprehensive mechanistic understanding of ultrasound-assisted extraction in phenolic-rich plant matrices and offers practical insights for the development of efficient and scalable extraction processes for natural-product-based industries.

2. METHODS

2.1. Materials

2.1.1. Raw materials

Soursop (*Annona muricata*) leaf powder was obtained from Nada Toserba Herbal (Jawa Barat, Indonesia). According to supplier information, the leaves were harvested from mature plants (approximately 2–3 years old) cultivated under tropical conditions and dried at room temperature (30–35 °C) before milling. To ensure raw material consistency, three commercial batches were initially screened based on total phenolic content (TPC), total flavonoid content (TFC), and antioxidant activity (IC_{50}). The batch showing the most stable phytochemical profile was selected as the standardized raw material for all experiments. The selected powder exhibited a moisture content of 4.43 ± 0.03% (wet basis) and was sieved to 500 µm using a vibratory sieve shaker (Retsch AS 200, Germany). After sieving, the powder was sealed in aluminum-laminated bags and stored at 4 °C in the dark to minimize oxidation and degradation of phenolic compounds prior to extraction. All experiments in this study used the same batch to maintain experimental reproducibility.

2.1.2. Chemicals

Analytical-grade solvents, including ethanol, methanol, and n-hexane, were purchased from Merck (Germany). Standards such as gallic acid, quercetin, aluminum chloride ($AlCl_3$), 2,2-diphenyl-1-picrylhydrazyl (DPPH), tannic acid, and quinine were obtained from Sigma–Aldrich (USA). Additional reagents used for phytochemical assays included Na_2CO_3, CH_3COOK, ascorbic acid, $FeCl_3$, vanillin–HCl reagent, Bromocresol Green (BCG), chloroform, diethyl ether, n-butanol, NaCl, acetic anhydride, and concentrated H_2SO_4. For instrumental analyses, potassium bromide (KBr) was used for FTIR measurements, helium was used as carrier gas for GC–MS, and methanol–water solutions (0.1% formic acid) were used for HPLC analysis. All chromatographic solvents were of HPLC grade (≥ 99.9% purity).

2.2. Extraction Methods

A schematic overview of the experimental workflow is shown in **Figure 1**, illustrating the sequence from raw material preparation, ultrasound-assisted extraction, Soxhlet extraction, extract concentration, kinetic modeling, and multi-analytical characterization.

DOI: https://doi.org/10.17509/ijost.v11i1.94654
p- ISSN 2528-1410 e- ISSN 2527-8045

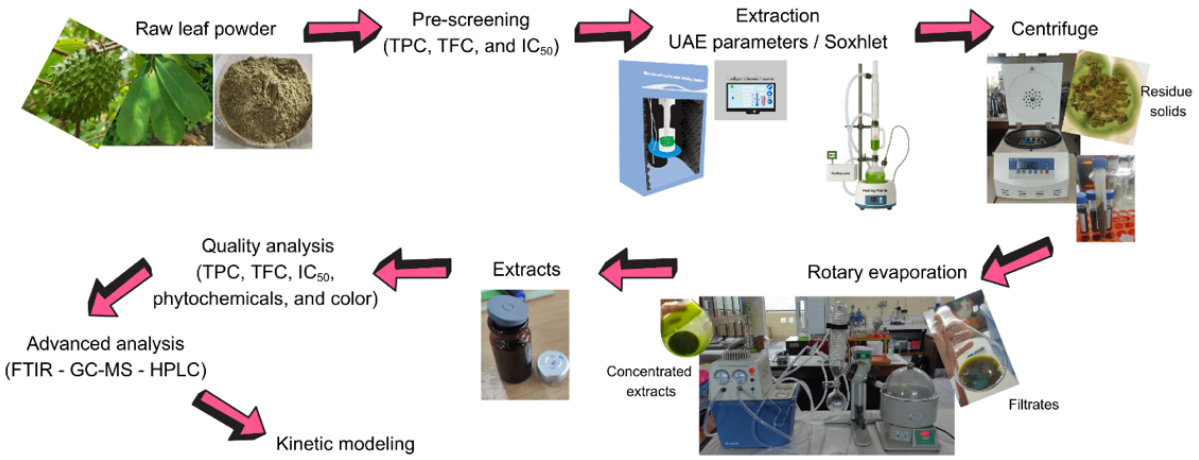

Figure 1. Experimental workflow of *Annona muricata* leaf extraction.

2.2.1. Ultrasound-assisted extraction (UAE)

Ultrasound-assisted extraction was performed using an ultrasonic processor (TUE-500, Toption, China) equipped with a 12 mm horn probe. Approximately 15 g of leaf powder was mixed with the extraction solvent at a solid-to-solvent ratio of 1:10 (w/v) in a glass beaker. Three ethanol–water solvent systems (100:0, 85:15, and 70:30 v/v) were investigated to represent different polarity environments for phenolic extraction. Ultrasonic power rates were set at 10%, 50%, and 90%, corresponding to low, medium, and high cavitation intensities. Extraction times ranged from 2.5 to 15 min to capture both the initial rapid extraction stage and the subsequent diffusion-controlled stage. The beaker was positioned 11 cm below the horn tip, with a 3.5 cm immersion depth, and the system was operated in pulsed mode (3 s ON/2 s OFF) to prevent excessive heating. The extraction temperature was maintained below 40 °C by intermittent cooling. After extraction, the mixture was centrifuged (B-ONE DC 6015-12, China) at 1000 rpm for 5 min, and the supernatant was collected for further analysis. All UAE experiments were conducted in triplicate (n = 3). The ranges of ultrasonic power, solvent ratios, and extraction times were selected based on preliminary screening experiments and previous studies reporting optimal UAE conditions for phenolic-rich plant matrices [1,6,7].

2.2.2. Soxhlet extraction

Conventional Soxhlet extraction was performed using a Soxhlet apparatus (HMC250, Joanlab, China) to serve as a benchmark for comparison with UAE. The same solid-to-solvent ratio (1:10 w/v) and solvent compositions used in the UAE were used to ensure methodological comparability. Approximately 15 g of leaf powder was placed in 8 × 10 cm non-woven extraction bags and inserted into the Soxhlet chamber. Extraction was conducted at 82–87 °C, with coolant temperature maintained at 10–20 °C. The number of extraction cycles was varied between 1 and 2, resulting in total extraction times of approximately 29–50 min. Each treatment was performed in triplicate.

2.2.3. Concentrated extracts

The collected filtrates were concentrated using a rotary evaporator (RE-2010VN, B-One, China) operated at 30 °C and 1000 rpm under reduced pressure (–0.09 to –0.10 MPa). The condenser temperature was maintained at 15–25 °C using a circulating vacuum pump system (B-One SHB-III). Evaporation was continued until no additional solvent condensate was

DOI: https://doi.org/10.17509/ijost.v11i1.94654
p- ISSN 2528-1410 e- ISSN 2527-8045

observed. To prevent oxidative degradation of phenolic compounds during storage, ascorbic acid (0.5% w/v) was added as an antioxidant stabilizer. The concentrated extracts were then transferred into amber vials and stored at –20 °C until further analysis.

2.3. Kinetic Modeling

2.3.1. Response parameters

Extraction efficiency was evaluated using three response indicators: extraction yield, yield-normalized total phenolic content (yield × TPC), and yield-normalized total flavonoid content (yield × TFC). These parameters were calculated using Eq. (1–2):

$$\text{yield}\ (\%) = \frac{V_{\text{filtrate}} \times C_{\text{filtrate}}}{m_{\text{powder}}} x\ 100\% \quad (1)$$

$$y_{TPC} = \text{yield} \times \text{TPC}, \qquad y_{TFC} = \text{yield} \times \text{TFC} \quad (2)$$

where $V_{filtrate}$ is the filtrate volume after rotary evaporation (mL), $C_{filtrate}$ is the extract concentration after rotary evaporation (g/mL), and m_{powder} is the initial mass of soursop leaf powder (g).

2.3.2. Mathematical models

Extraction kinetics were analyzed using several nonlinear models commonly used in solid–liquid extraction studies (**Table 1**). These models included polynomial models (Cubic, Poly 4, Poly 5), probabilistic models (Weibull, Gaussian peak, asymmetric Gaussian), and multi-peak models (Gaussian mixture, Gamma peak, and Ex-Gaussian). These models represent different extraction mechanisms, including rapid surface washing, cavitation-induced release, and diffusion-controlled extraction phases [13–15].

2.3.3. Model evaluation and validation

Model parameters were estimated using bounded nonlinear least squares regression (NLSR). Model performance was evaluated using the coefficient of determination (R^2) and root mean square error (RMSE) Eq. (3). Model selection was further supported by Akaike Information Criterion (AIC) and Bayesian Information Criterion (BIC) Eq. (4).

$$R^2 = 1 - \left(\frac{SSE}{TSS}\right),\ RMSE = \sqrt{\frac{SSE}{\sum n}},\ SSE = \sum_{i=1}^{n}\left(y_{exp,i} - y_{pre,i}\right)^2,\ TSS = \sum_{i=1}^{n}\left(y_{exp,i} - \overline{y_{exp,1}}\right)^2 \quad (3)$$

$$AIC = n \ln\left(\frac{SSE}{n}\right) + 2k, \quad BIC = n \ln(SSE) + k \ln(n) \quad (4)$$

Model robustness was evaluated using five-fold cross validation (k = 5) and residual analysis including runs tests and curvature diagnostics. A model was considered statistically adequate when $R^2 \geq 0.90$, RMSE ≤ 0.50, and AIC/BIC values were minimized.

Table 1. Model for the kinetics of extraction.

No	Model	Equation
1	Cubic	$y = p_1t^3 + p_2t^2 + p_3t + p_4$
2	Poly 4	$y = p_1t^4 + p_2t^3 + p_3t^2 + p_4t + p_5$
3	Poly 5	$y = p_1t^5 + p_2t^4 + p_3t^3 + p_4t^2 + p_5t + p_6$
4	Weibull	$y = a\left[1 - \exp\left\{-\left(\frac{t}{b}\right)^c\right\}\right]$

DOI: https://doi.org/10.17509/ijost.v11i1.94654
p- ISSN 2528-1410 e- ISSN 2527-8045

Table 1 (Continue). Model for the kinetics of extraction.

No	Model	Equation
5	Gaussian peak	$y = b + A\exp\left[-\frac{(t-\mu)^2}{2\sigma^2}\right]$
6	Asymmetric Gaussian	$y = b + A\exp\left[-\frac{(t-\mu)^2}{2\sigma^2_{L\text{ or }R}}\right]$
7	Gaussian mixture 2	$y = p_1\exp\left[-\frac{(t-p_2)^2}{2p_3^2}\right] + p_4\left[-\frac{(t-p_5)^2}{2p_6^2}\right] + p_7$
8	Gamma peak	$y = p_1 t^{(p_2-1)}\exp\left(-\frac{t}{p_3}\right) + p_4$
9	Ex-Gaussian	$y = b + A\, f_{exG}(t;\mu,\sigma,\tau)$ $f_{exG}(t;\mu,\sigma,\tau) = \frac{1}{2\tau}\exp\left(\frac{\sigma^2}{2\tau^2} - \frac{t-\mu}{\tau}\right)\mathrm{erfc}\left(\frac{\frac{\sigma^2}{\tau} - (t-\mu)}{\sqrt{2}\sigma}\right)$

Note: Cubic, Poly 4, and Poly 5 models = $p_1 - p_n$ are empirical coefficients; Weibull = a, b, c (the maximum value, time scale, and shape factor, respectively); Gaussian peak = A, μ, σ, b (amplitude, peak center (time), peak width, and baseline); asymmetric Gaussian, A, μ, σ_L, σ_R, b = amplitude, center, left/right width, and baseline; Gaussian mixture 2, p_1–p_6, p_7 = two Gaussian functions (amplitude, center, width) plus a baseline; Gamma peak, p_1–p_4 = amplitude, shape, time scale, and baseline Ex-Gaussian, A, μ, σ, τ, b = amplitude, Gaussian center, width, decay constant, and baseline.

All experimental data used for kinetic modelling were obtained from triplicate experiments, and mean values were used for model fitting.

2.4. Quality Analysis

2.4.1. Total phenolic compound (TPC)

TPC was quantified using a modified Folin–Ciocalteu method [16,17]. One milliliter of extract (10,000 ppm) was mixed with 2.5 mL of 10% Folin–Ciocalteu reagent, allowed to stand for 5 min, and then combined with 2 mL of 7.5% Na_2CO_3. After incubation for 30 min at 25 ± 2 °C in the dark, absorbance was measured at 765 nm (Shimadzu UV-1800). For raw/commercial powders, 1 g of sample was sonicated in 20 mL of 80% methanol for 30 min, filtered (0.45 µm) [18], and diluted to 1000 ppm before analysis. TPC was expressed as mg GAE/g using a gallic acid calibration curve. Calibration curves were constructed using five concentration levels (0–200 µg/mL), showing excellent linearity (R^2 > 0.99). All spectrophotometric analyses were performed in triplicate.

2.4.2. Total flavonoid compound (TFC)

TFC was determined using a modified aluminum chloride colorimetric method [19]. One milliliter of extract (10,000 ppm) was mixed with 0.2 mL of 1 M CH_3COOK, 0.2 mL of 10% $AlCl_3$, and 5.6 mL of distilled water, then incubated for 30 min at 25 ± 2 °C. Absorbance was measured at 415 nm. TFC was expressed as mg QE/g using a quercetin calibration curve constructed using five concentration levels (0–200 µg/mL) with R^2 > 0.99. Sample preparation for raw materials and commercial powders followed the TPC protocol. Three randomly selected extracts were further analyzed for IC_{50}, quantitative phytochemicals (total tannins, total alkaloids, total saponins, total steroids), color (L, a*, b*), FTIR, GC–MS, and HPLC.

2.4.3. Antioxidant activity (IC_{50})

Radical scavenging capacity was assessed using DPPH, following modified methods by Baliyan et al. [20] and Gulcin & Alwasel [21]. Two milliliters of extract (1000 ppm) were mixed

DOI: https://doi.org/10.17509/ijost.v11i1.94654
p- ISSN 2528-1410 e- ISSN 2527-8045

with 2 mL of 0.1 mM DPPH solution, incubated for 30 min in the dark at 25 ± 2 °C, and the absorbance was measured at 517 nm. Inhibition (%) was calculated using Eq. (5):

$$\text{Inhibition (\%)} = \frac{A_0 - A_1}{A_0} \times 100 \quad (5)$$

where A_0 is the absorbance of the control, and A_1 is the absorbance of the sample. IC_{50} was determined from the inhibition (%) versus concentration plot. Sample preparation followed the TPC procedure.

2.4.4. Total tannins

Total tannins were quantified using a modified vanillin–HCl assay with tannic acid as the standard [22]. One milliliter of extract (1000 ppm) was mixed with 5 mL vanillin–HCl reagent, incubated for 30 min at 25 ± 2 °C, and the absorbance was read at 500 nm. Results were expressed as mg tannic acid equivalents per gram (mg TAE/g) using a 0.1–10 mg/mL calibration curve.

2.4.5. Total alkaloids

Total alkaloids were measured using a modified Bromocresol Green (BCG) method [23]. Briefly, one milliliter of extract (1000 ppm) was reacted with BCG reagent and 5 mL of chloroform, and vortexed. The chloroform layer was separated and measured at 470 nm. Results were expressed as mg quinine equivalents per gram (mg QE/g).

2.4.6. Total saponins

Total saponins were determined following modified protocols [24,25]. The extract was re-extracted with water: ethanol (1:4), reduced to 40 mL, and partitioned with diethyl ether. The aqueous phase was then extracted with 60 mL n-butanol, washed with 5% NaCl, and the butanol phase was evaporated. Saponin content was expressed as % w/w.

2.4.7. Total steroids

Total steroids were measured using a modified Liebermann–Burchard colorimetric method [26]. One milliliter of extract (1000 ppm) was mixed with 2 mL chloroform and 2 mL acetic anhydride, followed by 1 mL concentrated H_2SO_4 to develop a bluish-green color. Absorbance was measured at 620 nm and quantified using a cholesterol calibration curve (mg/g).

2.4.8. Color parameters (L, a*, b*)

Color parameters were measured using a HunterLab ColorFlex EZ colorimeter (USA) in accordance with CIE standards [27,28]. Undiluted extracts were analyzed and total color difference (ΔE) was calculated using Eq. (6):

$$\Delta E = \sqrt{(L_2 - L_1)^2 + (a_2^* - a_1^*)^2 + (b_2^* - b_1^*)^2} \quad (6)$$

2.4.9. FTIR analysis

FTIR spectra were recorded using a PerkinElmer Spectrum Two UATR spectrometer (USA) over 4000–400 cm^{-1}, with 4 cm^{-1} resolution and 32 scans/sample. Samples (extracts, powders, and commercial products) were analyzed directly on the ATR crystal (n = 3), and spectra were baseline-corrected and normalized. Key bands for lignocellulosic–phenolic structures were

DOI: https://doi.org/10.17509/ijost.v11i1.94654
p- ISSN 2528-1410 e- ISSN 2527-8045

identified. Index ratios such as crystallinity (A_{1420}/A_{895}), phenolic/aromatic (A_{1600}/A_{1420}), glycosidic (A_{1045}/A_{1150}), and aliphatic (A_{1508}/A_{1630}) were calculated [29,30]. Peak shifts in the O–H in Eq. (7) were interpreted as red/blue shift linked to hydrogen bonding and amorphization [31]:

$$\Delta\nu_{(OH)} = \nu_{OH,\ sample} - \nu_{OH,\ fresh} \tag{7}$$

2.4.10. GC-MS analysis

Volatile compounds were analyzed using a Shimadzu GCMS–TQ8050 NX (Japan) with a DB-5MS column (30 m × 0.25 mm × 0.25 µm). Key parameters: injector 260 °C, helium flow 1.49 mL/min, and splitless mode. Oven profile: 60 °C (1 min) → 200 °C (1 min) → 260 °C (2 min) at 5 °C/min. Ion source: 220 °C, interface: 250 °C. Mass range: m/z 33–1000 at 5000 scans/s with an acquisition time of 0.2 s, and solvent cut was set at 2 min. A 1 µL aliquot of evaporated extract was injected. Compounds were identified via NIST 17 and Wiley Registry libraries (≥ 85% match).

2.4.11. HPLC analysis

Non-volatile phenolic compounds were analyzed using a Shimadzu LC-20AD HPLC system (Japan) equipped with a photodiode array detector (PDA) and a C18 column (250 mm × 4.6 mm, 5 µm). The mobile phase consisted of methanol:water (70:30 v/v) delivered in isocratic mode at 1.0 mL/min. Column temperature was maintained at 30 °C, and detection was performed at 370 nm. Samples were diluted with ethanol (1:3), dissolved in methanol (1 mg/mL), filtered through a 0.45 µm PTFE membrane, and injected in a 10 µL volume. Quantification of quercetin was performed using an external calibration curve constructed from five standard concentrations. The method showed excellent linearity (R^2 > 0.995). Results were expressed as µg/mL of liquid extract using Eq. (8):

$$C_{sample} = \frac{A_{sample}}{A_{std}} \times C_{std} \tag{8}$$

where A_{sample} is the sample area, A_{std} is the quercetin standard area, and C_{std} is the concentration of quercetin standard. Method precision was evaluated by triplicate injections, producing relative standard deviation (RSD < 5%). Limits of detection (LOD) and quantification (LOQ) were estimated using signal-to-noise ratios of 3:1 and 10:1, respectively, confirming the method's suitability for quantitative analysis of quercetin in plant extracts.

2.5. Statistical Analysis and Software

All experiments were performed in triplicate (n = 3), and results are reported as mean ± standard deviation. For UAE experiments, three-way ANOVA was used to evaluate the effects of ultrasonic power rate, solvent ratio, and extraction time, followed by Tukey's post hoc test ($p < 0.05$) in Minitab 21 (USA). Soxhlet extraction data were analyzed using two-way ANOVA, while phytochemical and antioxidant data were evaluated using one-way ANOVA. Effect sizes were calculated using Cohen's d with pooled standard deviation. Extraction kinetic modeling was conducted using MATLAB R2025[a] (MathWorks, USA). Correlations between GC–MS peak area percentages and antioxidant activity or phenolic recovery were evaluated using Pearson correlation analysis.

DOI: https://doi.org/10.17509/ijost.v11i1.94654
p- ISSN 2528-1410 e- ISSN 2527-8045

3. RESULTS AND DISCUSSION

3.1. Yield of *Annona muricata* Leaf Extraction

Ultrasound-assisted extraction (UAE) was evaluated under different ultrasonic power rates (10–90%), ethanol–water ratios (100:0–70:30), and extraction times (2.5–15 min). Three-way ANOVA confirmed that all main factors and their interactions significantly influenced extraction yield ($p < 0.001$; **Table 2**), indicating that extraction performance was controlled by the combined effects of solvent polarity and cavitation intensity. Yield increased rapidly during the initial stage of extraction and reached a maximum within approximately 5–7.5 min (**Figure 2a**), after which it gradually declined, suggesting the onset of degradation under prolonged cavitation exposure [32,33]. Among the tested solvents (**Figure 2b**), the 70:30 ethanol–water mixture consistently yielded the highest yields, demonstrating that semi-polar hydroalcoholic media enhance the dissolution of phenolic-rich constituents while maintaining efficient mass transfer [34,35]. The influence of ultrasonic power rate showed a non-linear pattern: increasing power from 10% to 50% improved extraction yield due to stronger cavitation, whereas excessive intensity (90%) reduced yield at longer extraction times due to localized heating and degradation of thermolabile compounds [36,37]. These trends indicate that efficient UAE requires a balance between solvent polarity and cavitation intensity to maximize compound release while preserving extract stability.

Under the optimal region identified in the interaction analysis (70:30 solvent ratio, ~50% ultrasonic power, and 5–7.5 min extraction), UAE produced yields of approximately 3.6–4.1%, whereas Soxhlet extraction yielded 0.77–3.49% under comparable solvent conditions (**Figure 2c**). This corresponds to an approximate 17–368% improvement in extraction yield, depending on solvent ratio and extraction cycle. The higher performance of the UAE is attributed to cavitation-induced microjets and shockwaves generated during bubble collapse, which disrupt plant cell walls and accelerate solvent penetration into intracellular structures [1,6]. These mechanical effects enhance diffusion of phenolic compounds from the lignocellulosic matrix, whereas Soxhlet extraction relies primarily on slower solvent recirculation and conductive heating. Similar yield improvements have been reported in UAE studies of phenolic-rich plant matrices, where cavitation can increase extraction efficiency by 20–60% while reducing extraction time from hours to minutes [6,7]. From a practical perspective, the rapid extraction time (≤7.5 min) suggests that UAE could substantially reduce processing time and energy consumption compared with conventional Soxhlet extraction, highlighting its potential for scalable industrial extraction of bioactive compounds.

Table 2. ANOVA on yield of extraction.

Source	DF	Adj SS	Adj MS	F-value	P-value	Partial η^2
A	2	1.2505	0.6252	1278563.31	< 0.001	0.999920
B	2	47.2201	23.6101	48280996.80	< 0.001	0.999998
C	5	7.2542	1.4508	2966884.16	< 0.001	0.999986
A × B	4	3.9173	0.9793	2002664.33	< 0.001	0.999974
A × C	10	5.8160	0.5816	1189323.09	< 0.001	0.999983
B × C	10	7.3360	0.7336	1500153.10	< 0.001	0.999986
A × B × C	20	14.6386	0.7319	1496747.99	< 0.001	0.999993
Error	108	0.0001	0.00018			
Total	161	87.4327				

Note: A = power rate, B = ratio ethanol:water, and C = time. All effects significant at $p < 0.001$ (Tukey's test). Partial $\eta^2 > 0.99$ indicates very strong effect size.

DOI: https://doi.org/10.17509/ijost.v11i1.94654
p- ISSN 2528-1410 e- ISSN 2527-8045

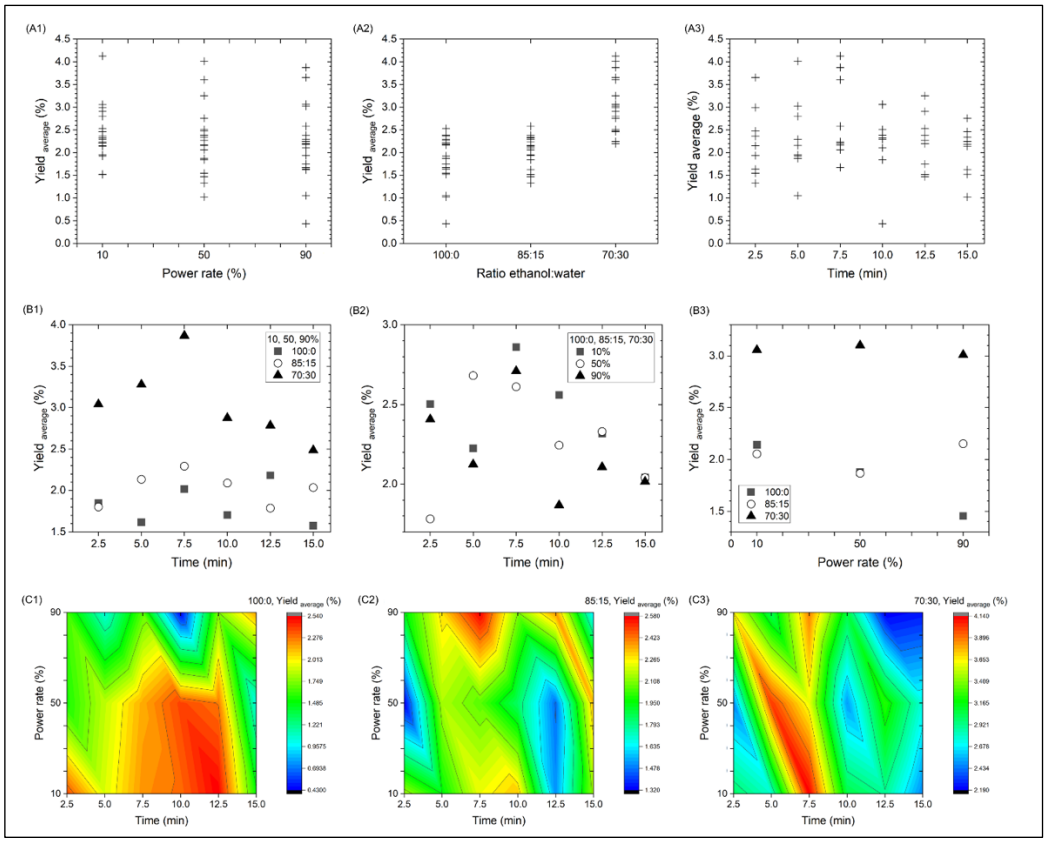

Figure 2. Yield of extraction: (a) one, (b) two, and (c) three-way interaction.

3.2. Yield × TPC of *Annona muricata* Leaf Extraction

Within the hierarchical evaluation framework proposed in this study, extraction yield represents the quantity of extract obtained, whereas yield × TPC reflects the efficiency of phenolic compound recovery, integrating extraction quantity with phenolic concentration. This indicator therefore provides a more meaningful measure of extraction performance than yield alone because it directly reflects the recovery of antioxidant-active phenolics from the plant matrix [36]. Three-way ANOVA confirmed that ultrasonic power rate, solvent ratio, extraction time, and their interactions significantly affected yield × TPC ($p < 0.001$; **Table 3**). The extraction profile showed a rapid increase during the early extraction stage and reached a maximum at approximately 5–7.5 min before gradually declining (**Figure 3a**). This behavior indicates that phenolic release initially benefits from cavitation-induced cell disruption and enhanced solvent penetration. However, prolonged ultrasonic exposure may promote oxidative degradation of phenolic molecules through radical formation generated during cavitation bubble collapse. In addition, localized micro-heating produced by cavitation events may destabilize thermolabile phenolic structures and accelerate oxidation reactions. Consequently, an optimal extraction window exists where cavitation improves mass transfer without causing excessive degradation of phenolic compounds.

The interaction plots further indicated that the most favorable UAE region occurred at a 70:30 ethanol–water solvent ratio combined with moderate ultrasonic power rate (≈50%) and extraction times near 5 min, producing the highest yield × TPC values among the evaluated treatments (**Figure 3b** and **Figure 3c**). Hydroalcoholic solvents have frequently been reported to enhance phenolic recovery in medicinal plants because the mixed polarity improves solubility of both free phenolics and glycosylated derivatives while maintaining efficient diffusion from plant tissues [38–40]. Similar trends have been observed in UAE studies on

DOI: https://doi.org/10.17509/ijost.v11i1.94654
p- ISSN 2528-1410 e- ISSN 2527-8045

phenolic-rich matrices such as *Moringa oleifera* and *Rosmarinus officinalis*, where moderate ultrasonic intensity maximized phenolic extraction while preventing degradation associated with excessive cavitation [1,39]. In contrast, Soxhlet extraction produced lower yield × TPC values despite longer extraction times (**Table 4** and **Figure 4a**), suggesting that prolonged thermal exposure may accelerate phenolic oxidation and reduce antioxidant-active compounds [41,42]. Although commercial products contained higher absolute phenolic concentrations due to industrial concentration processes, UAE demonstrated competitive phenolic recovery when normalized by extraction time and energy input. These findings highlight that yield × TPC functions as the second-level indicator in the extraction hierarchy, bridging extraction quantity (yield) with functional phenolic recovery. The optimized phenolic extraction conditions identified here therefore provide a mechanistic basis for evaluating flavonoid recovery using the yield × TFC indicator in the following section.

Table 3. ANOVA on yield × TPC of extraction.

Source	DF	Adj SS	Adj MS	F-value	P-value	Partial η^2
A	2	20.79	10.397	561703.83	< 0.001	0.999995
B	2	1770.82	885.408	47833056.8	< 0.001	1.000000
C	5	138.87	27.774	1500458.84	< 0.001	0.999999
A × B	4	42.42	10.604	572882.64	< 0.001	0.999998
A × C	10	174.23	17.423	941234.9	< 0.001	0.999999
B × C	10	177.09	17.709	956706.64	< 0.001	0.999999
A ×B × C	20	415.91	20.795	1123442.37	< 0.001	1.000000
Error	108	0.0001	0.00012			
Total	161	2740.12				

Note: A = power rate, B = ratio ethanol:water, and C = time. All effects significant at $p < 0.001$ (Tukey's test). Partial $\eta^2 > 0.99$ indicates very strong effect size.

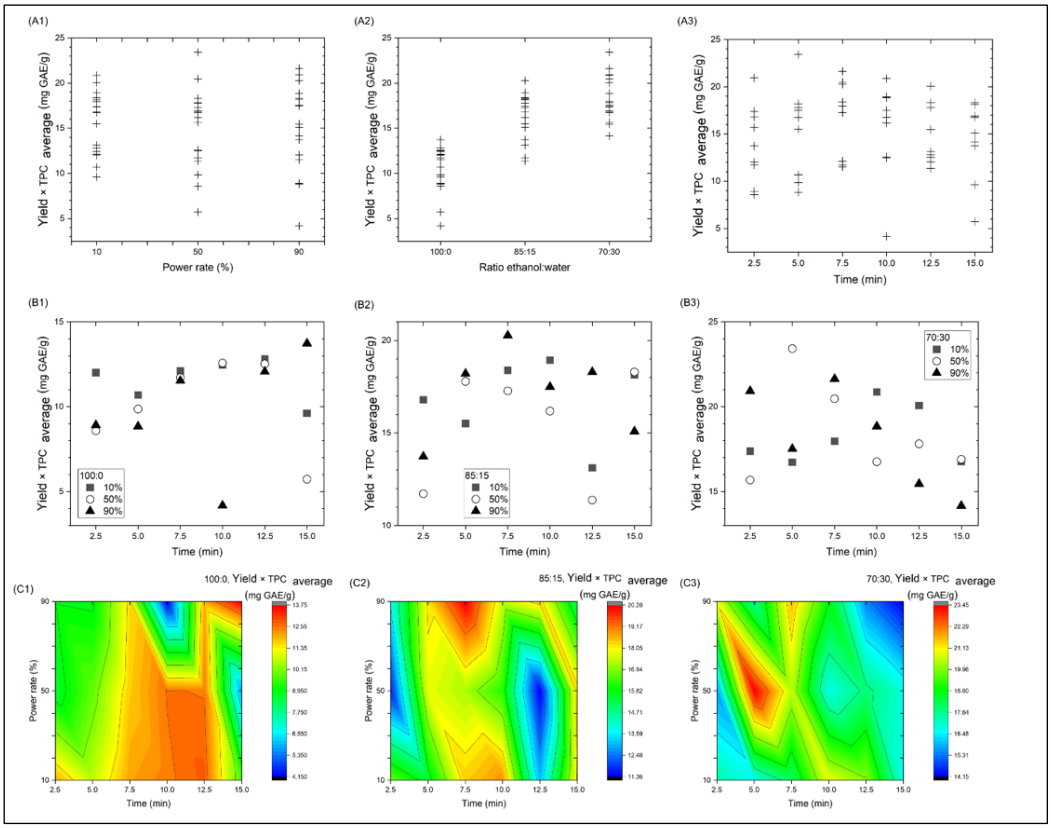

Figure 3. Yield × TPC of extraction: (a) one, (b) two, and (c) three-way interaction.

DOI: https://doi.org/10.17509/ijost.v11i1.94654
p- ISSN 2528-1410 e- ISSN 2527-8045

Table 4. ANOVA on yield × TPC of Soxhlet extraction.

Source	DF	Adj SS	Adj MS	F-value	P-value	Partial η^2
B	2	26.003	13.0015	2054850.85	< 0.001	0.999996
D	1	76.157	76.1571	12036449.92	< 0.001	0.999999
B × D	2	89.232	44.6158	7051424.11	< 0.001	0.999999
Error	12	0.0001	0.00014			
Total	17	191.392				

Note: B = ratio ethanol:water, and D = cycle time. All effects significant at $p < 0.001$ (Tukey's test). Partial η^2 values > 0.99 indicate extremely strong effect sizes.

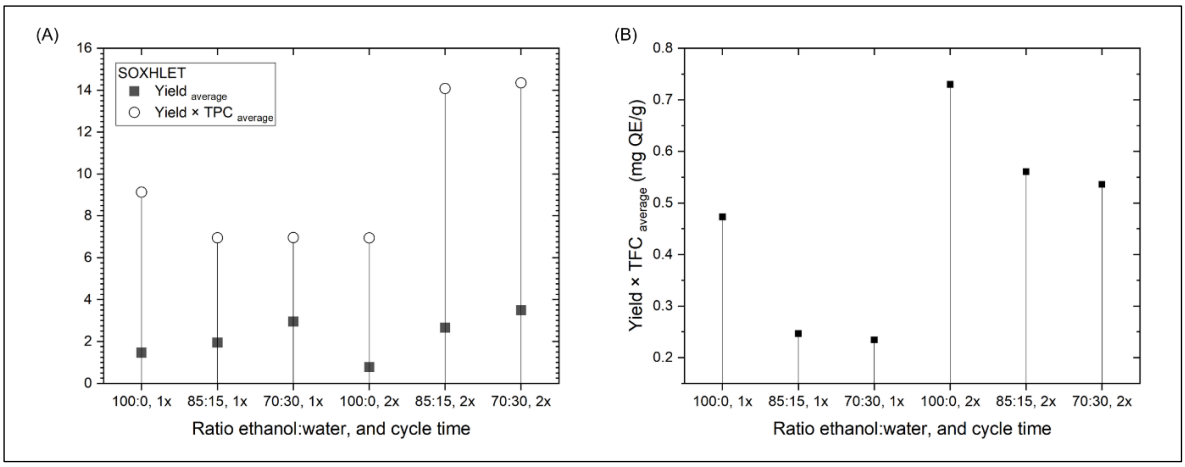

Figure 4. Soxhlet extraction: (a) yield and yield × TPC, and (b) yield × TFC.

3.3. Yield × TFC of *Annona muricata* Leaf Extraction

The yield-normalized total flavonoid content (yield × TFC) was evaluated to determine whether the extraction conditions that maximized phenolic recovery also promoted flavonoid release. Three-way ANOVA confirmed that ultrasonic power rate, solvent ratio, extraction time, and their interactions significantly influenced yield × TFC ($p < 0.001$; **Table 5**). Unlike yield × TPC, which reached its maximum under a 70:30 ethanol–water ratio, the highest yield × TFC values were generally observed with the 85:15 solvent system (**Figure 5**). This difference can be attributed to the polarity characteristics of flavonoids, many of which occur as glycosides that exhibit intermediate polarity and therefore dissolve more efficiently in moderately polar solvents rather than highly aqueous systems [43,44]. In addition, excessive water content may promote hydrolysis or oxidative degradation of flavonoid glycosides during ultrasonic processing, reducing their stability compared with phenolic acids [12]. Consequently, the slightly less polar 85:15 solvent environment appears to provide a more favorable balance between solubility and chemical stability for flavonoid compounds.

The extraction profile also reflected differences in the release mechanism of flavonoids from plant tissues. Many flavonoids are partially bound to lignocellulosic cell-wall structures or occur as glycosylated derivatives that require stronger cavitation-induced disruption to be released into the solvent phase [45,46]. As a result, yield × TFC tended to reach its maximum at slightly longer extraction times than yield × TPC, indicating a slower diffusion stage associated with cell-wall disintegration and cleavage of weak intermolecular interactions. The response to ultrasonic power rate was therefore non-linear: moderate cavitation enhanced cell-wall rupture and mass transfer, whereas excessive ultrasonic intensity increased the likelihood of oxidative degradation of flavonoid structures [47]. Compared with Soxhlet extraction (**Table 6** and **Figure 4b**), UAE achieved higher flavonoid recovery within a significantly shorter extraction period, highlighting the advantage of cavitation-driven

DOI: https://doi.org/10.17509/ijost.v11i1.94654
p- ISSN 2528-1410 e- ISSN 2527-8045

extraction over conventional thermal solvent recirculation [48,49]. Overall, these results indicate that an ethanol–water ratio near 85:15 combined with moderate ultrasonic intensity provides optimal conditions for releasing flavonoids while preserving their structural stability.

Table 5. ANOVA on yield × TFC of extraction.

Source	DF	Adj SS	Adj MS	F-value	P-value	Partial η^2
A	2	34.559	17.2797	121389000	< 0.001	0.999997
B	2	23.968	11.984	84187056.18	< 0.001	0.999996
C	5	80.991	16.1981	113791000	< 0.001	0.999999
A × B	4	59.508	14.8771	104511000	< 0.001	0.999998
A × C	10	157.558	15.7558	110684000	< 0.001	0.999999
B × C	10	150.092	15.0092	105439000	< 0.001	0.999999
A × B × C	20	300.874	15.0437	105682000	< 0.001	1.000000
Error	108	0.0001	0.00011			
Total	161	807.551				

Note: A = power rate, B = ratio ethanol:water, and C = time. All effects significant at $p < 0.001$ (Tukey's test). Partial $\eta^2 > 0.99$ indicates very strong effect size.

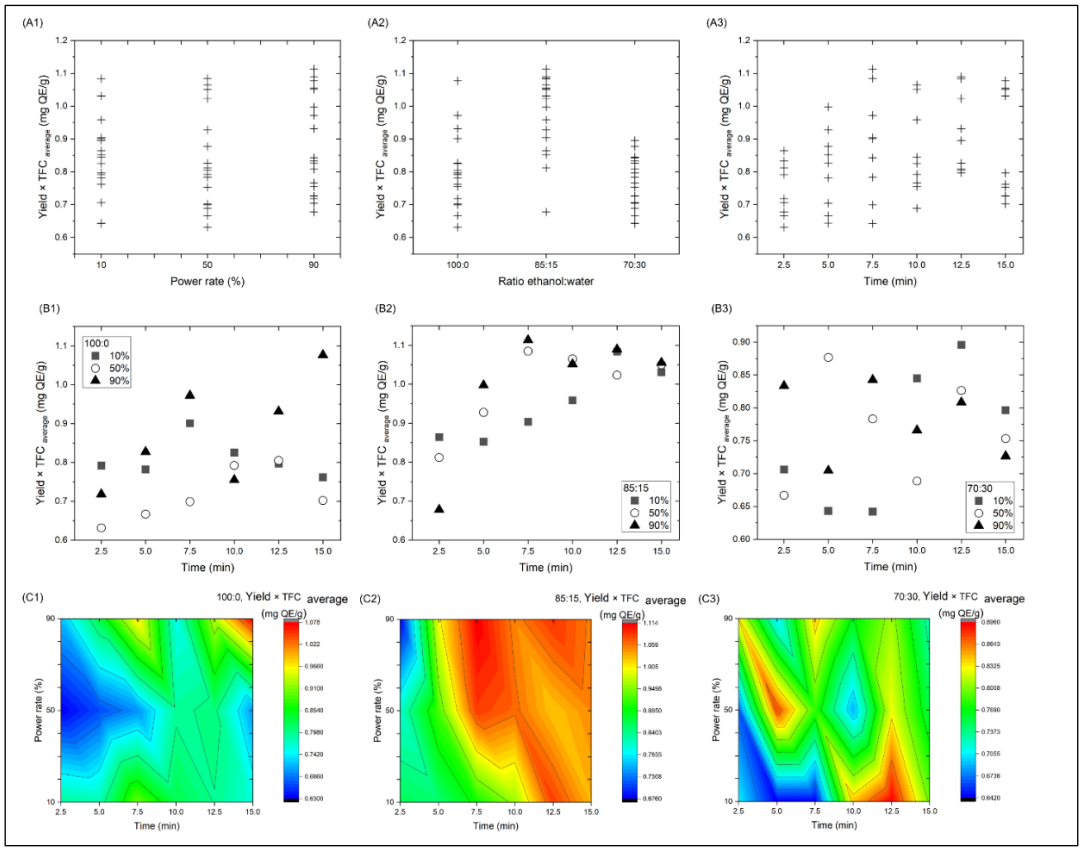

Figure 5. Yield × TFC of extraction: (a) one, (b) two, and (c) three-way interaction.

Table 6. ANOVA on yield × TFC of Soxhlet extraction.

Source	DF	Adj SS	Adj MS	F-value	P-value	Partial η^2
B	2	0.172529	0.086265	7210103.42	< 0.001	0.999421
D	1	0.380898	0.380898	31835952.01	< 0.001	0.999738
B × D	2	0.002696	0.001348	112678.05	< 0.001	0.964235
Error	12	0.0001	0.00012			
Total	17	0.556124				

Note: A = power rate, B = ratio ethanol: water, and C = time. All effects significant at $p < 0.001$ (Tukey's test). Partial $\eta^2 > 0.99$ indicates a very strong effect size.

DOI: https://doi.org/10.17509/ijost.v11i1.94654
p- ISSN 2528-1410 e- ISSN 2527-8045

3.4. Extraction Kinetics of *Annona muricata* Leaf

Kinetic modeling was conducted to clarify the extraction dynamics underlying the trends observed for yield, yield × TPC, and yield × TFC during ultrasound-assisted extraction. Unlike many UAE studies that apply a single empirical model, the present work evaluated multiple kinetic models—including polynomial, Weibull-type, and probabilistic distributions—to better capture the different physical mechanisms governing bioactive release from plant matrices (**Tables 7 to 9**). This multi-model strategy enables the extraction process to be interpreted in terms of both mass-transfer behavior and cavitation-induced structural disruption, thereby linking extraction kinetics to bioactive recovery efficiency. In general, the UAE profiles exhibited a two-stage extraction pattern consisting of an initial fast-release phase followed by a slower diffusion-controlled stage, which is typical for solid–liquid extraction of lignocellulosic plant tissues [50,51]. The early stage is dominated by cavitation-induced cell-wall rupture and microstreaming, which accelerate solvent penetration and release of readily accessible compounds. Subsequently, extraction becomes controlled by diffusion of intracellular compounds through partially disrupted cell walls. By integrating kinetic modelling with the hierarchical indicators used in Sections 3.1–3.3, the analysis provides a mechanistic framework linking cavitation intensity, solvent polarity, and bioactive compound recovery. This approach therefore extends previous UAE studies by explicitly relating kinetic behavior to phenolic and flavonoid extraction efficiency.

3.4.1. Kinetics of extraction yield

The extraction yield profile increased rapidly during the early stage of UAE and reached a maximum at approximately 5–7.5 min before gradually declining at longer extraction times. This behavior reflects the balance between enhanced mass transfer induced by cavitation and the potential degradation of thermolabile compounds under prolonged ultrasonic exposure. Model fitting showed that both mixture-type probabilistic models and higher-order polynomial models were able to describe this non-linear trajectory depending on extraction conditions (**Table 7**). For example, the Gaussian mixture 2 model captured the coexistence of two kinetic regimes corresponding to the rapid surface-washing stage and the subsequent slower diffusion phase (**Figure 6a**). In contrast, polynomial models described the smooth curvature of the extraction trajectory near the maximum yield. These findings indicate that the extraction yield is controlled by a dynamic interaction between cavitation-induced cell-wall disruption and diffusion-limited solute transport [11,52]. The results therefore confirm that moderate ultrasonic intensity promotes efficient mass transfer while preventing excessive thermal degradation.

Although the Poly 5 model produced very high statistical fits under several extraction conditions, the risk of overfitting associated with high-order polynomial models must be considered. Polynomial models provide flexible curve fitting, but their coefficients generally lack direct physical interpretation compared with probabilistic models such as Weibull functions [53]. Therefore, model evaluation in this study did not rely solely on R^2 values but also considered RMSE, AIC/BIC criteria, and residual behavior to ensure statistical robustness and model parsimony. Under optimal UAE conditions (70:30 solvent ratio and moderate ultrasonic power), the fitted kinetic curves indicated a rapid, cavitation-driven release followed by stabilization near the equilibrium yield. This pattern suggests that solvent polarity and cavitation intensity jointly determine the efficiency of cell-wall disruption and solute diffusion. Consequently, kinetic modeling confirms the extraction mechanism proposed in Section 3.1, where moderate cavitation intensity provides the most favorable balance between mass transfer enhancement and compound stability.

DOI: https://doi.org/10.17509/ijost.v11i1.94654
p- ISSN 2528-1410 e- ISSN 2527-8045

3.4.2. Kinetics of extraction yield × TPC

The kinetic behavior of yield × TPC showed a clear maximum at intermediate extraction times, indicating that phenolic recovery initially increased but declined under prolonged cavitation exposure. This pattern reflects the rapid desorption of loosely bound phenolics followed by slower diffusion of compounds associated with cell-wall structures [51,54]. Among the evaluated models, the Poly 4 model provided the most appropriate compromise between statistical accuracy and structural simplicity for the optimal UAE condition (**Table 8** and **Figure 6b**). Compared with Weibull or probabilistic models, Poly 4 produced lower RMSE and more stable residual distributions while avoiding the excessive parameterization associated with higher-order polynomial functions. The resulting kinetic curves indicate that phenolic extraction is initially controlled by cavitation-enhanced mass transfer but gradually becomes diffusion-limited as readily accessible phenolics are depleted. In addition, the hydro-alcoholic solvent system (70:30 ethanol–water) produced a smoother kinetic trajectory than absolute ethanol, suggesting that solvent polarity improves both phenolic solubility and diffusion within the plant matrix. These results demonstrate that kinetic modeling can help explain why the semi-polar solvent system produced the highest phenolic recovery observed in Section 3.2.

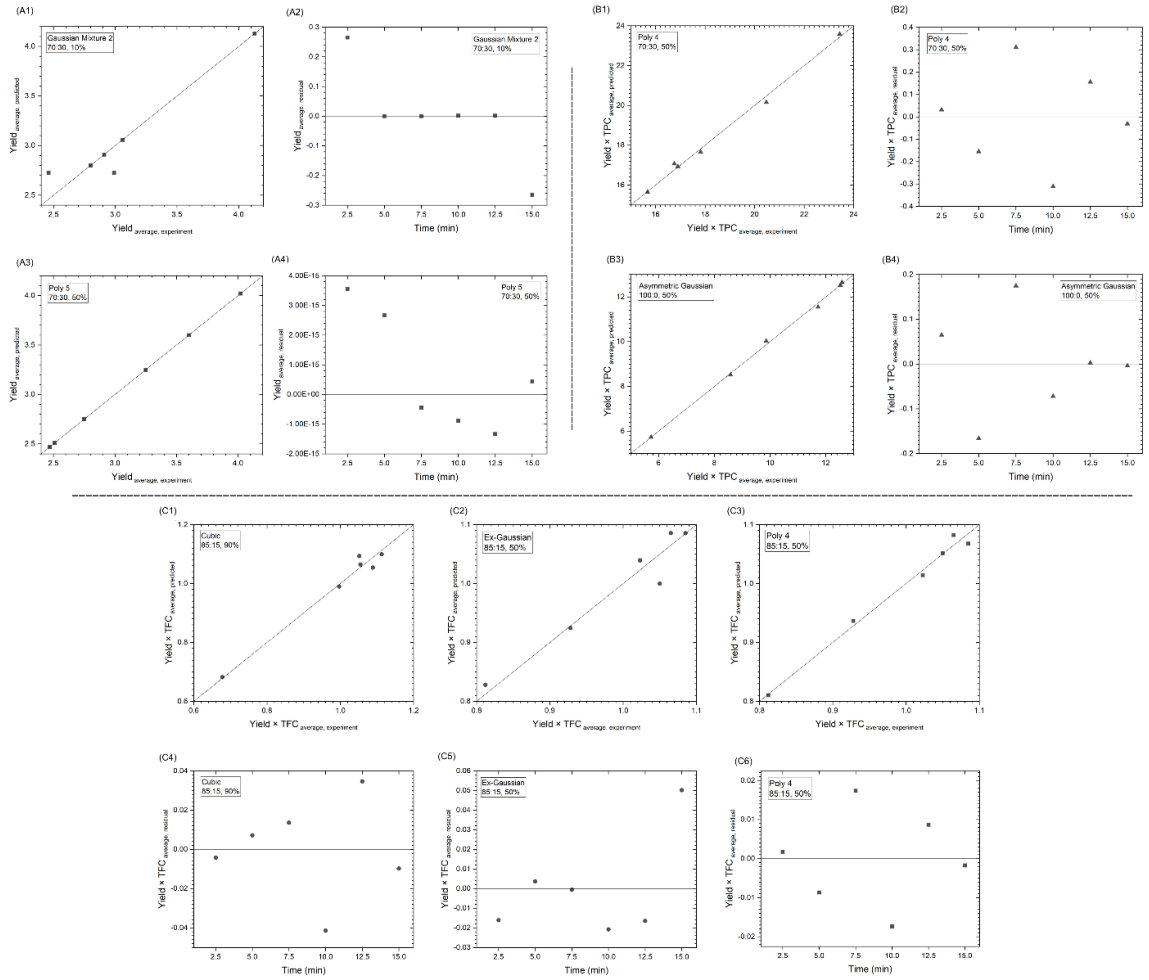

Figure 6. Extraction kinetics model for: (a) yield, (b) yield × TPC, and (c) yield × TFC.

DOI: https://doi.org/10.17509/ijost.v11i1.94654
p- ISSN 2528-1410 e- ISSN 2527-8045

3.4.3. Kinetics of extraction yield × TFC

Flavonoid extraction exhibited a kinetic pattern similar to that observed for phenolics but with a slightly delayed maximum. This difference is consistent with the stronger structural association of flavonoids with lignocellulosic cell-wall components or glycosidic linkages, which require more extensive cavitation-induced disruption to be released [46,55]. Consequently, the kinetic curves showed a prolonged diffusion stage before reaching the peak flavonoid recovery. Among the evaluated models, the Poly 4 model again provided the best compromise between goodness of fit and parameter parsimony (**Table 9** and **Figure 6c**). Probabilistic models such as Ex-Gaussian functions were able to represent asymmetric extraction curves, but they did not significantly improve predictive performance compared with Poly 4. These results indicate that flavonoid release during UAE is primarily governed by gradual matrix disruption, followed by diffusion-limited transport of glycosylated flavonoids. Therefore, the kinetic behavior of flavonoids supports the interpretation that moderate cavitation intensity is required to effectively liberate structurally bound compounds from plant tissues.

3.4.4. Model selection and interpretation

The final selection of kinetic models was based on a combination of statistical performance and physical interpretability (**Table 1**). Although high-order polynomial models often produced extremely high R^2 values, simpler models with fewer parameters may provide more realistic representations of diffusion-controlled extraction processes [53,56]. Therefore, the selected models were required to simultaneously satisfy multiple evaluation criteria, including low RMSE, favorable AIC/BIC values, and stable residual distributions. This multi-criteria approach reduces the risk of overfitting while ensuring that the kinetic model remains consistent with the physical mechanisms governing extraction. Several experimental limitations should also be considered when interpreting these results. First, a 2.5 min time resolution may not fully capture the very early burst-release stage immediately after ultrasound exposure. Second, cavitation intensity within ultrasonic systems may exhibit spatial heterogeneity, which can influence local mass-transfer conditions. Third, variations in particle size distribution and internal plant structure may contribute to variability in diffusion pathways. Despite these limitations, the modeling results consistently demonstrate that solvent polarity and cavitation intensity jointly regulate extraction kinetics and bioactive compound recovery during UAE.

3.5. Antioxidant Activity, Phytochemicals, and Color

The functional quality of the extracts was further evaluated through antioxidant activity, phytochemical composition, and color stability to determine whether the extraction trends observed for yield, yield × TPC, and yield × TFC were reflected in the extracts. Three representative UAE extracts (R100, R85, and R70) were selected and compared with the bioactivities of the Soxhlet extract, raw material, and commercial samples (**Tables 10–11** and **Figure 7**). In general, extracts obtained under semi-polar solvent environments exhibited stronger antioxidant activity than those obtained using absolute ethanol or prolonged thermal extraction. This behavior reflects the enhanced recovery of phenolic and flavonoid compounds in hydroalcoholic systems, which are widely recognized as the primary contributors to radical-scavenging activity in plant extracts [57]. Because phenolic compounds possess multiple hydroxyl groups capable of donating hydrogen atoms or electrons, their presence directly influences the antioxidant capacity of plant-derived extracts. Consequently,

DOI: https://doi.org/10.17509/ijost.v11i1.94654
p- ISSN 2528-1410 e- ISSN 2527-8045

extraction conditions that preserve phenolic integrity are critical for maintaining extract bioactivity. The UAE treatments that produced higher phenolic recovery therefore tended to generate extracts with stronger antioxidant performance.

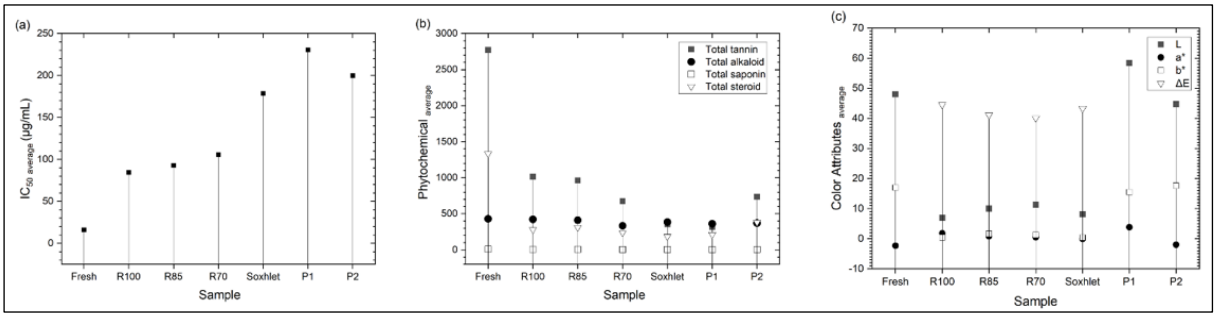

Figure 7. Antioxidant activity, phytochemicals, and color.

The relationship between phenolic content and antioxidant activity can be explained by the hydrogen atom transfer (HAT) and single-electron transfer (SET) mechanisms, which are commonly involved in phenolic radical-scavenging reactions. In these mechanisms, phenolic hydroxyl groups donate hydrogen atoms or electrons to stabilize reactive free radicals such as DPPH, forming resonance-stabilized phenoxyl radicals [11]. As a result, extracts with higher phenolic concentrations typically exhibit lower IC_{50} values, indicating stronger antioxidant capacity. The trends observed in this study therefore support the strong functional link between phenolic recovery (yield × TPC) and antioxidant performance. Similar correlations between phenolic concentration and radical scavenging activity have been widely reported in ultrasound-assisted extraction of medicinal plants [58]. These results indicate that the enhanced cavitation-induced release of phenolics during UAE directly contributes to improved antioxidant functionality.

Phytochemical analysis further demonstrated that different compound groups exhibit varying stability during extraction: total alkaloids > total saponins > total tannins ≳ total steroids. High-molecular-weight phenolics such as tannins were the most sensitive to processing conditions, likely due to depolymerization or oxidative reactions during ultrasonic or thermal treatment [59]. In contrast, alkaloids showed relatively minor variations among treatments, suggesting that nitrogen-containing heterocyclic structures are more stable under cavitation conditions. Saponins exhibited moderate reductions that may be associated with partial hydrolysis or structural rearrangements during extraction. Steroidal compounds were the most sensitive to prolonged heating, indicating that excessive thermal exposure may alter sterane-type molecular structures [60]. These observations highlight that extraction conditions influence not only the quantity of recovered compounds but also the stability of different phytochemical classes.

Color measurements provided additional evidence of chemical transformations occurring during extraction. All extracts showed noticeable color differences compared with the raw material, reflecting pigment degradation and oxidation reactions occurring during processing. However, UAE extracts obtained under semi-polar solvent systems exhibited smaller color changes than Soxhlet extracts, indicating better preservation of pigment-associated phenolic compounds. Phenolics are known to inhibit oxidative browning reactions by scavenging reactive oxygen species and stabilizing intermediate radicals [61]. The observed relationship between antioxidant activity and color stability therefore supports the protective role of phenolic compounds in maintaining extract quality. From an application perspective, these findings suggest that UAE-derived extracts could serve as promising functional ingredients for nutraceutical, pharmaceutical, or natural antioxidant formulations. The ability of UAE to

DOI: https://doi.org/10.17509/ijost.v11i1.94654
p- ISSN 2528-1410 e- ISSN 2527-8045

produce phenolic-rich extracts within a short processing time therefore highlights its potential as an efficient and scalable extraction strategy for natural-product-based industries.

3.6. Fourier Transform Infrared (FTIR) Analysis

FTIR spectroscopy was used to examine structural modifications of the *Annona muricata* leaf matrix induced by different extraction conditions. The spectra displayed characteristic absorption bands associated with lignocellulosic and phenolic structures, including broad O–H stretching vibrations at 3200–3300 cm^{-1}, aliphatic C–H stretching around 2920–2850 cm^{-1}, aromatic C=C vibrations near 1600 cm^{-1}, and carbohydrate-related C–O/C–O–C bands within the 1200–1000 cm^{-1} region (**Figure 8**). These functional groups are typical of phenolic-rich plant matrices and provide insight into structural transformations occurring during extraction [29,30]. Compared with the raw material, UAE extracts showed noticeable variations in peak intensity and band positions, indicating disruption of lignocellulosic structures caused by ultrasonic cavitation. Such structural changes increase solvent accessibility and facilitate the release of intracellular bioactive compounds. The spectroscopic evidence therefore supports the higher extraction efficiency observed under UAE conditions compared with Soxhlet extraction.

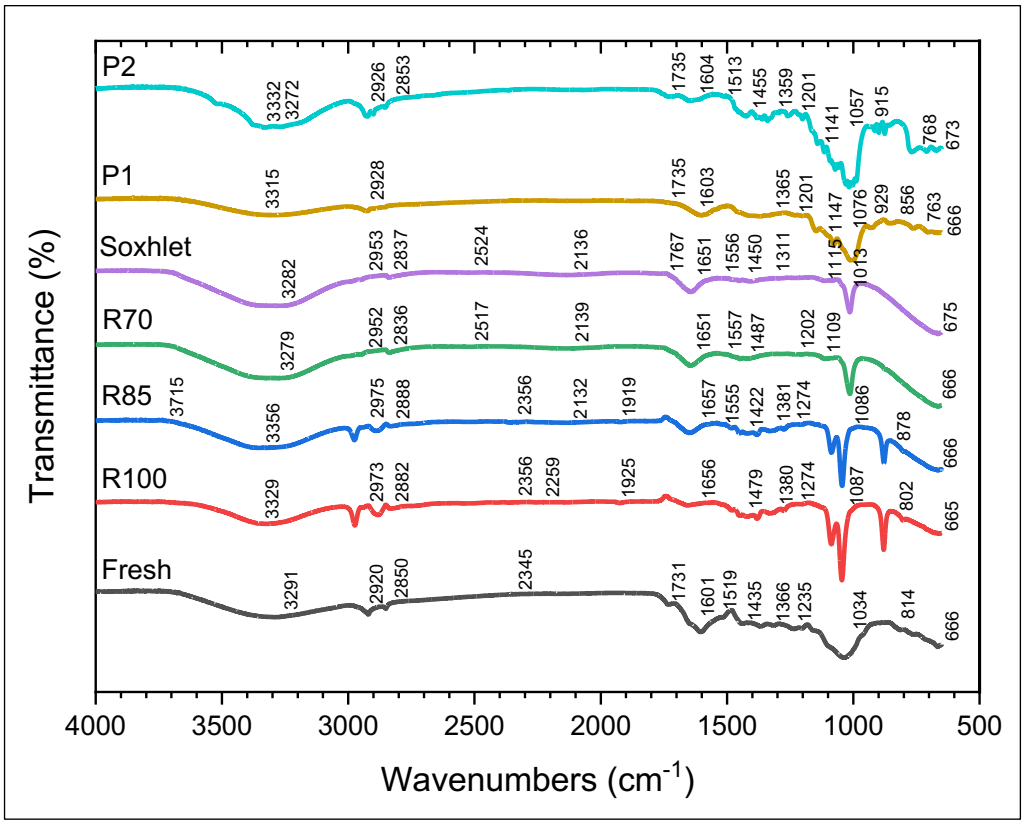

Figure 8. FTIR spectra of soursop leaf powder extraction.

To further interpret matrix modification, several spectroscopic indices were evaluated (**Figure 9**), including the crystallinity index (CI) and phenolic/aromatic index (PAI). Extracts obtained under conditions that produced higher yield × TPC values generally exhibited lower crystallinity indices, indicating partial amorphization of ordered lignocellulosic structures. This phenomenon reflects cavitation-induced mechanical disruption of plant cell walls, which enhances solvent penetration and promotes phenolic diffusion from intracellular compartments [29,30]. Conversely, treatments showing higher CI values corresponded to lower phenolic recovery, suggesting limited structural disruption of the plant matrix. These

DOI: https://doi.org/10.17509/ijost.v11i1.94654
p- ISSN 2528-1410 e- ISSN 2527-8045

findings demonstrate that spectroscopic indicators of matrix accessibility correlate with the extraction efficiency trends reported in Sections 3.1–3.3. Consequently, FTIR provides structural evidence linking cavitation intensity with enhanced phenolic release during UAE.

Within the integrated analytical framework of this study, FTIR serves as the first step for understanding extraction mechanisms by revealing cavitation-induced structural changes in the plant matrix. Structural disruption observed in FTIR spectra explains the enhanced liberation of phytochemicals subsequently detected by chromatographic techniques. GC–MS analysis (Section 3.7) identifies volatile and semi-volatile compounds released from the disrupted matrix, while HPLC analysis (Section 3.8) quantifies specific flavonoid markers such as quercetin. The complementary use of these techniques therefore enables structural, compositional, and quantitative aspects of the extraction process to be interpreted within a unified analytical framework. This integrated interpretation provides mechanistic insight into how ultrasound-assisted extraction modifies plant matrices and improves bioactive compound recovery.

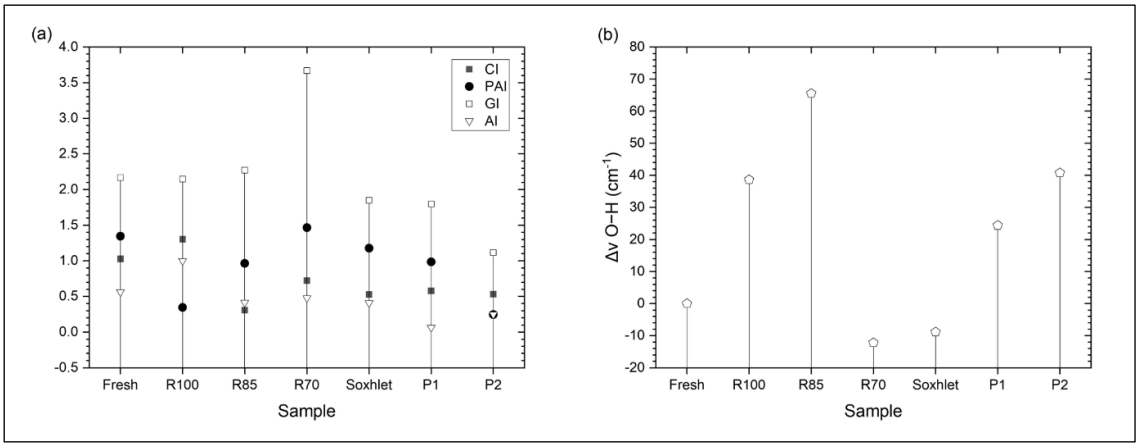

Figure 9. Spectroscopic index of soursop leaf powder extraction.

3.7. Gas Chromatography–Mass Spectrometry (GC-MS) Analysis

GC–MS analysis was performed to characterize volatile and semi-volatile phytochemicals in *Annona muricata* leaf extracts and to assess how extraction conditions influence chemical composition (**Table 12**). The chromatographic profiles revealed multiple compounds belonging to phenolic derivatives, terpenoids, fatty acids, and ester compounds, which are frequently reported in soursop leaves and contribute to their biological activity [62,63]. Among the detected compounds, several oxygenated molecules, such as quinic-acid-related derivatives and phenolic aromatic compounds, were observed in UAE extracts. These compounds are known intermediates in plant phenolic metabolism and may contribute to antioxidant properties through hydrogen-donating and radical-stabilizing mechanisms [64]. The presence of these oxygenated molecules indicates that ultrasound cavitation facilitates the release of intracellular metabolites from plant tissues by disrupting lignocellulosic cell-wall structures. This mechanism is consistent with the FTIR evidence presented in Section 3.6, which suggested cavitation-induced structural modification of the plant matrix. Therefore, GC–MS results provide complementary molecular evidence supporting the enhanced extraction efficiency observed under UAE conditions.

The phytochemical profiles also differed depending on solvent polarity and cavitation intensity. Extracts obtained using semi-polar ethanol–water systems contained relatively higher proportions of oxygenated aromatic compounds and phenolic derivatives, whereas extracts produced with absolute ethanol were comparatively richer in terpenoid and ester

DOI: https://doi.org/10.17509/ijost.v11i1.94654
p- ISSN 2528-1410 e- ISSN 2527-8045

compounds. Such differences reflect the role of solvent polarity in determining the solubility of plant metabolites and the efficiency of mass transfer during extraction [64]. One of the compounds detected in several UAE extracts was phytol, a diterpenoid alcohol derived from chlorophyll degradation that has been reported to possess antioxidant and antimicrobial activity [65]. The presence of phytol suggests that cavitation not only releases phenolic compounds but may also liberate lipid-derived metabolites from chlorophyll-containing tissues. Similar GC–MS profiles have been reported in previous studies of *A. muricata* leaves, where phytol, fatty acid derivatives, and oxygenated aromatic compounds were identified as dominant components of the volatile fraction [62,63]. These results demonstrate that UAE influences both the quantity and the qualitative composition of extracted phytochemicals.

The GC–MS results were further interpreted in relation to antioxidant activity measured in Section 3.5 (**Figure 10**). Extracts enriched in oxygenated aromatic and phenolic-related compounds generally corresponded to samples exhibiting stronger radical-scavenging activity, indicating that phenolic molecules play a dominant role in determining antioxidant performance. Phenolic compounds are known to stabilize free radicals through electron or hydrogen atom donation from hydroxyl functional groups, thereby inhibiting oxidative chain reactions [64]. In contrast, extracts dominated by aliphatic or lipid-derived molecules tended to exhibit weaker antioxidant capacity, suggesting that these compounds contribute less to radical-scavenging activity. This relationship confirms that extraction efficiency should not be interpreted solely based on total extract yield, but rather on the recovery of bioactive phenolic molecules. Nevertheless, GC–MS primarily detects volatile and semi-volatile compounds; therefore, non-volatile phenolics may be underrepresented in the chromatographic profile. For this reason, complementary chromatographic techniques such as HPLC are required to accurately quantify major flavonoid markers in the extracts. Consequently, the following section focuses on HPLC quantification of quercetin as a representative flavonoid compound in *A. muricata* leaf extracts.

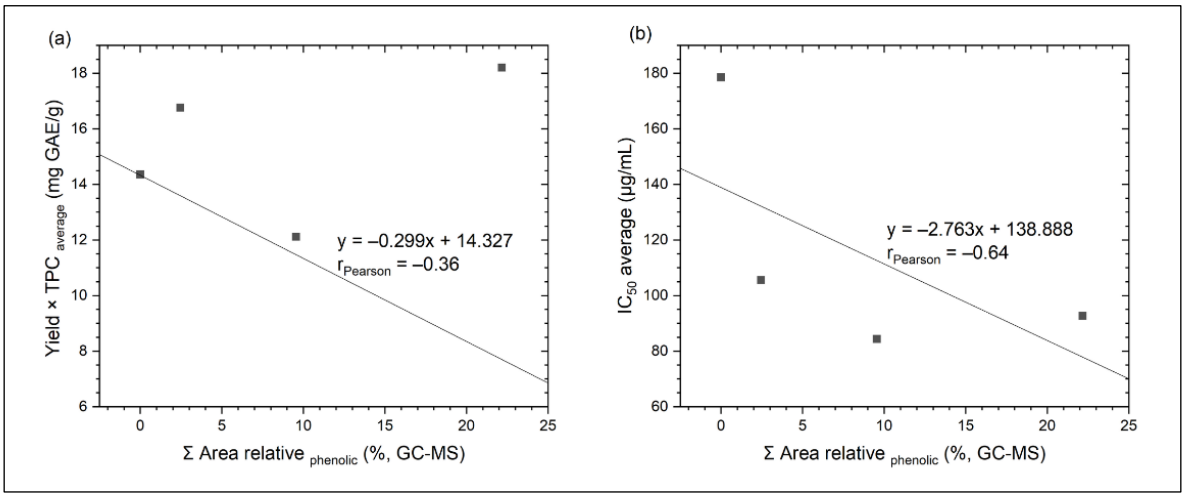

Figure 10. Pearson correlation between relative and: (a) yield × TPC, and (b) IC_{50}.

3.8. High Performance Liquid Chromatography (HPLC) Analysis

High-performance liquid chromatography (HPLC) was used to confirm the presence of quercetin as a representative flavonoid marker in *Annona muricata* leaf extracts (**Figure 11**). The quercetin standard exhibited a characteristic retention time of approximately 4.8 min, which served as the identification reference for chromatographic comparison with the extract samples. The calibration curve showed excellent linearity (R^2 > 0.995) across the tested

DOI: https://doi.org/10.17509/ijost.v11i1.94654
p- ISSN 2528-1410 e- ISSN 2527-8045

concentration range, while replicate injections produced relative standard deviation (RSD) values below 5%, indicating satisfactory analytical repeatability. These parameters confirm that the HPLC method reliably quantifies quercetin in the extracts. Chromatographic results revealed that detectable quercetin peaks were observed primarily in UAE extracts obtained with hydroalcoholic solvent systems, indicating that solvent polarity strongly influences the release of flavonoid aglycones from the plant matrix. This observation supports the extraction trends observed for yield × TFC in Section 3.3, where semi-polar solvent systems enhanced flavonoid recovery. The selective detection of quercetin under these conditions therefore reflects the ability of ultrasound-assisted extraction to liberate flavonoids through cavitation-induced disruption of cell-wall structures.

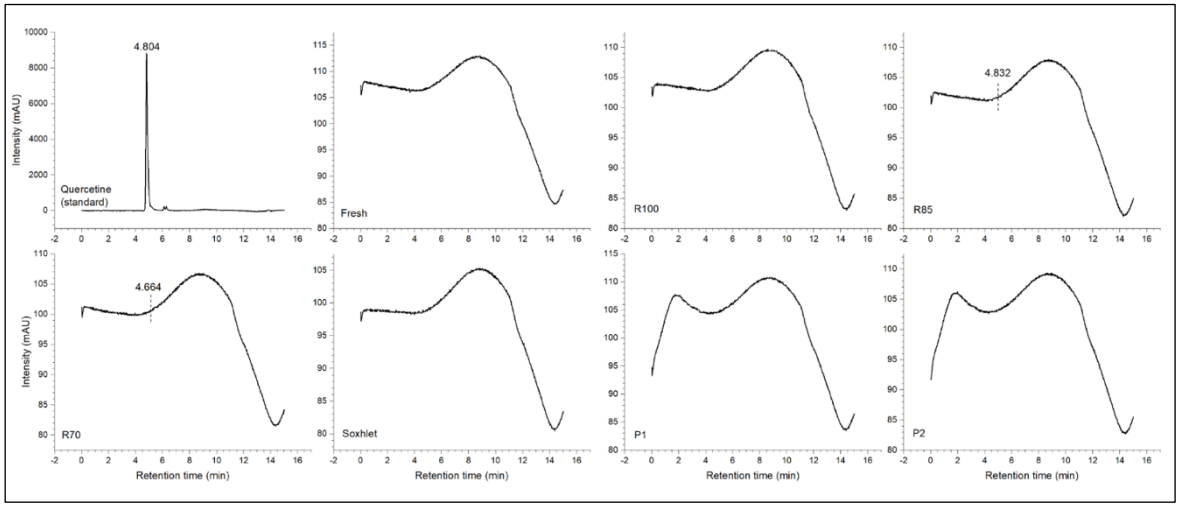

Figure 11. Chromatograms for the quercetin standard and all extract samples.

In addition to quercetin, several additional chromatographic peaks were detected, indicating the presence of other phenolic constituents commonly reported in *A. muricata* leaves, including phenolic acids and flavonoid derivatives such as rutin and quinic acid metabolites [66,67]. These findings are consistent with the GC–MS results discussed in Section 3.7, which identified phenolic derivatives as major chemical components in the extracts. In many plant matrices, flavonoids occur predominantly as glycosylated forms rather than as free aglycones and therefore may not be fully detected under the isocratic HPLC conditions used in this study [68]. Consequently, the relatively moderate quercetin peak intensity observed in some extracts does not necessarily indicate low flavonoid content but may instead reflect the presence of glycosylated derivatives. This interpretation aligns with the earlier results for total flavonoid content, suggesting that flavonoid recovery involves a complex mixture of aglycone and glycoside forms. The combined chromatographic evidence, therefore, confirms that UAE conditions capable of maximizing yield × TFC also promote the release of specific flavonoid molecules.

The presence of quercetin was also consistent with the antioxidant activity trends discussed in Section 3.5. Extracts containing detectable quercetin peaks generally exhibited stronger radical-scavenging capacity, reflecting the well-known ability of flavonoid hydroxyl groups to donate hydrogen atoms and stabilize reactive radicals [69,70]. However, antioxidant activity cannot be attributed solely to quercetin, as plant extracts typically contain complex mixtures of phenolic compounds that act synergistically. Synergistic interactions among flavonoids and phenolic acids are known to enhance overall antioxidant activity through complementary redox mechanisms. Therefore, quercetin should be interpreted primarily as a representative marker of flavonoid-rich extracts rather than the sole

DOI: https://doi.org/10.17509/ijost.v11i1.94654
p- ISSN 2528-1410 e- ISSN 2527-8045

determinant of antioxidant capacity. Because the HPLC method used in this study mainly detects aglycone forms, further studies employing gradient HPLC or LC–MS analysis would be required to comprehensively characterize flavonoid glycosides. Overall, the chromatographic results support the integrated analytical framework of this study by linking extraction conditions, flavonoid recovery, and antioxidant functionality at the molecular level.

4. CONCLUSION

This study demonstrates that ultrasound-assisted extraction (UAE) provides a significantly more efficient approach than Soxhlet extraction for recovering bioactive compounds from *Annona muricata* leaves, producing extraction yields of approximately 3.6–4.1% compared with 0.77–3.49% for Soxhlet, corresponding to an improvement of roughly 17–368% under comparable solvent conditions. Beyond a simple comparison of extraction methods, the present work introduces a hierarchical evaluation framework comprising three indicators—yield (extraction quantity), yield × TPC (phenolic recovery), and yield × TFC (flavonoid recovery)—that enables extraction efficiency to be interpreted systematically across different levels of bioactive recovery. Kinetic modelling further revealed a characteristic two-stage extraction mechanism consisting of rapid cavitation-induced release followed by diffusion-controlled transport. The integration of complementary analytical techniques provides mechanistic insight into this process: FTIR reveals cavitation-induced disruption of the lignocellulosic plant matrix, GC–MS identifies the volatile and semi-volatile metabolites released from the disrupted tissues, and HPLC quantifies quercetin as a representative flavonoid marker associated with antioxidant functionality. Together, these analyses bridge the previously limited understanding of the connections among extraction efficiency, plant-matrix structural modification, and phytochemical composition in UAE studies of medicinal plants. From a practical perspective, the short extraction time (≤7.5 min) and improved phenolic recovery indicate that UAE has strong potential as a scalable, energy-efficient technology for the industrial production of natural antioxidant extracts. Nevertheless, several limitations should be acknowledged, including the relatively coarse kinetic time resolution, potential spatial heterogeneity in cavitation intensity in ultrasonic systems, and the limited detection of flavonoid glycosides with the isocratic HPLC method used in this study. Future research should therefore focus on pilot-scale UAE optimization, advanced LC–MS/MS characterization of phenolic compounds, development of mechanistic diffusion–cavitation kinetic models, and evaluation of extract stability for nutraceutical and pharmaceutical applications.

5. ACKNOWLEDGMENTS

The authors acknowledged the financial support from Universitas Diponegoro 2025.

6. AUTHORS' NOTE

The authors declare that there is no conflict of interest regarding the publication of this article. The authors confirmed that the paper was free of plagiarism and that an AI proofreader (ChatGPT-4o) was used to assist in the proofreading process.

7. REFERENCES

[1] Nolasco-González, Y., Chacón-López, M. A., Ortíz-Basurto, R. I., Aguilera-Aguirre, S., González-Aguilar, G. A., Rodríguez-Aguayo, C., Navarro-Cortez, M. C., García-Galindo, H.

S., García-Magaña, M. D. L., Meza-Espinoza, L., and Montalvo-González, E. (2022). *Annona muricata* leaves as a source of bioactive compounds: Extraction and quantification using ultrasound. *Horticulturae*, *8*(7), 560.

[2] Santos, R. K. da S., Silva, R. A. da, Ferreira, M. R. A., Soares, L. A. L., Stragevitch, L., and Danielski, L. (2022). *Annona muricata* leaf extracts obtained with subcritical water and conventional methods: evaluation of antioxidant activities, total polyphenol and rutin contents. *Acta Scientiarum Technology*, *45*, e61153.

[3] Kamal, A. A. A., Mohamad, M., Masri, M. N., Ter, T. P., Shoparwe, N. F., and Lim, J. W. (2023). Comparison of quercetin yield obtained using convectional and ultrasound-assisted extraction from *Chromolaena odorata*. *AIP Conference Proceedings*, 030012.

[4] Lee, C. H., Lee, T. H., Ong, P. Y., Wong, S. L., Hamdan, N., Elgharbawy, A. A. M., and Azmi, N. A. (2021). Integrated ultrasound-mechanical stirrer technique for extraction of total alkaloid content from *Annona muricata*. *Process Biochemistry*, *109*, 104–116.

[5] Sari, D. A., Djaeni, M., Prasetyaningrum, A., and Sasongko, S. B. (2025). Extraction techniques and optimization strategies for phytochemicals from *Annona muricata* leaf: A comprehensive review (2010-2024). *International Journal of Agriculture and Biology*, *34*(1), 1–13.

[6] Aguilar-Villalva, R., Molina, G. A., España-Sánchez, B. L., Díaz-Peña, L. F., Elizalde-Mata, A., Valerio, E., Azanza-Ricardo, C., and Estevez, M. (2021). Antioxidant capacity and antibacterial activity from *Annona cherimola* phytochemicals by ultrasound-assisted extraction and its comparison to conventional methods. *Arabian Journal of Chemistry*, *14*(7), 103239.

[7] Wang, L., Sun, Z., Wang, L., and Tian, S. (2024). Optimization of ultrasonic-assisted extraction of polyphenols from *Salvia deserta* Schang flowers based on response surface methodology and deep neural network and analysis of its in vitro antioxidant activities. *Industrial Crops and Products*, *213*, 118389.

[8] Daghaghele, S., Kiasat, A. R., Ardebili, S. M. S., and Mirzajani, R. (2021). Intensification of extraction of antioxidant compounds from *Moringa oleifera* leaves using ultrasound-assisted approach: BBD-RSM design. *International Journal of Fruit Science*, *21*(1), 693–705.

[9] Diwathe, M. C., and Mazumdar, B. (2024). Optimization of ultrasound-assisted extraction of phenolics from *Cordia dichotoma* leaves using response surface methodology. *Chemical Engineering Research and Design*, *208*, 572–587.

[10] Adilah, Z. A. M., Hanani, Z. A. N., Ezzat, M. A., Asma, A. R. N., and Noranizan, M. A. (2024). Impact of ultrasound-assisted extraction on physical properties, antioxidant activity, and colorimetric pH-response of blackcurrant pomace extract. *ACS Food Science and Technology*, *4*(11), 2645–2654.

[11] Lozano-Puentes, H. S., Sánchez-Matiz, J. J., Ruiz-Sanchez, E., Costa, G. M., and Díaz-Ariza, L. A. (2023). *Guadua angustifolia* Kunth leaves as a source for bioactive phenolic compounds: Optimization of ultrasound-assisted extraction using response surface methodology and antioxidant activities. *Heliyon*, *9*(12), e22445.

[12] Hartati, R., Rompis, F., Pramastya, H., and Fidrianny, I. (2024). Optimization of antioxidant activity of soursop (*Annona muricata* L.) leaf extract using response surface methodology. *Biomedical Reports*, *21*(5), 166.

[13] Mahfud, M., Nabila, A. R., and Variyana, Y. (2025). Developing a kinetic model for microwave hydro diffusion and gravity with steam flow on extraction of essential oils from *Amomum compactum* seeds. *Rasayan Journal of Chemistry*, *18*(1), 52–60.

[14] Mui, M., Ruben, R. M., Ricker, T. J., Dobryakova, E., and Sandry, J. (2022). Ex-Gaussian

DOI: https://doi.org/10.17509/ijost.v11i1.94654
p- ISSN 2528-1410 e- ISSN 2527-8045

analysis of simple response time as a measure of information processing speed and the relationship with brain morphometry in multiple sclerosis. *Multiple Sclerosis and Related Disorders*, *63*, 103890.

[15] Wang, Y., Yang, S., Bao, G., and Wang, H. (2024). Pyrolysis of macadamia nut peel using multicomponent Gaussian kinetic modeling and ANN analysis. *Biomass and Bioenergy*, *183*, 107170.

[16] Pérez, M., Dominguez-López, I., and Lamuela-Raventós, R. M. (2023). The chemistry behind the Folin–Ciocalteu method for the estimation of (poly)phenol content in food: Total phenolic intake in a Mediterranean dietary pattern. *Journal of Agricultural and Food Chemistry*, *71*(46), 17543–17553.

[17] Utari, F. D., Sari, D. A., Kurniasari, L., Kumoro, A. C., Djaeni, M., and Hii, C.-L. (2023). The enhancement of sappanwood extract drying with foaming agent under different temperature. *AIMS Agriculture and Food*, *8*(1), 214–235.

[18] Sari, D. A., Djaeni, M., Susanti, D. Y., Karyadi, J. N. W., Hutabarat, O. S., Sasongko, S. B., Prasetyaningrum, A., and Hii, C.-L. (2026). Development and comparison of drying tropical herbal srategies for *Annona muricata* leaves: Integrating of effective moisture diffusivity using antioxidant activity, FTIR ratios, and color attributes. *Trends in Sciences*, *23*(6), 12279.

[19] Nurlinda, N., Handayani, V., and Rasyid, F. A. (2021). Spectrophotometric determination of total flavonoid content in biancaea sappan (*Caesalpinia sappan* L.) leaves. *Jurnal Fitofarmaka Indonesia*, *8*(3), 1–4.

[20] Baliyan, S., Mukherjee, R., Priyadarshini, A., Vibhuti, A., Gupta, A., Pandey, R. P., and Chang, C.-M. (2022). Determination of antioxidants by dpph radical scavenging activity and quantitative phytochemical analysis of *Ficus religiosa*. *Molecules*, *27*, 1326.

[21] Gülçin, İ., and Alwasel, S. H. (2023). DPPH radical scavenging assay. *Processes*, *11*(8), 2248.

[22] Herald, T. J., Gadgil, P., Perumal, R., Bean, S. R., and Wilson, J. D. (2014). High-throughput micro-plate HCl–vanillin assay for screening tannin content in sorghum grain. *Journal of the Science of Food and Agriculture*, *94*(10), 2133–2136.

[23] Elchamieh, S., Jaber, A., Ibrahim, G., and Cheble, E. (2024). Spectrophotometric and chromatographic determination of alkaloids and nicotine contents in Lebanese tobacco leaves. *Yüzüncü Yıl Üniversitesi Tarım Bilimleri Dergisi*, *34*(2), 335–345.

[24] Adeku, E., Osundahunsi, O. F., Malomo, S. A., Asasile, I. I., Owolabi, O. M., and Oyewole, G. (2022). Phytochemical constituents and assessment of crude extracts from *Boerhavia diffusa* L. and *Lonchocarpus sericeus* (Poir.) Kunth ex DC. leaves for antioxidant and antibacterial activities. *Measurement: Food*, *5*, 100018.

[25] Obadoni, B. O., and Ochuko, P. O. (2002). Phytochemical studies and comparative efficacy of crude extracts of some homeostatic plants in Edo and Delta States of Nigeria. *Global Journal of Pure and Applied Sciences*, *8*(2), 203–208.

[26] Adu, J. K., Amengor, C. D. K., Kabiri, N., Orman, E., Patamia, S. A. G., and Okrah, B. K. (2019). Validation of a simple and robust Liebermann–Burchard colorimetric method for the assay of cholesterol in selected milk products in Ghana. *International Journal of Food Science*, *2019*, 1–7.

[27] Altay, K., Dirim, S. N., and Hayaloglu, A. A. (2024). Effects of different drying processes on the quality changes in Arapgir purple basil (*Ocimum basilicum* L.) leaves and drying-induced changes in bioactive and volatile compounds and essential oils. *Journal of Food Science*, *89*(12), 9088–9107.

[28] Kumar, G., J. J. T., Rao, P. S., and Manchikanti, P. (2023). Effect of thin layer drying

DOI: https://doi.org/10.17509/ijost.v11i1.94654
p- ISSN 2528-1410 e- ISSN 2527-8045

conditions on the retention of bioactive components in Malabar spinach (*Basella alba*) leaves. *Food Chemistry Advances*, *3*, 100419.

[29] Gong, Q., Guo, Z., Sun, Z., Gong, J., and Wei, F. (2020). Graphene oxide-assisted ethanol reflux extraction of total flavonoids from *Ginkgo biloba* leaves: Study of kinetics and mechanism. *Chemical Papers*, *74*(3), 971–984.

[30] Lomovskiy, I., Makeeva, L., Podgorbunskikh, E., and Lomovsky, O. (2020). The influence of particle size and crystallinity of plant materials on the diffusion constant for model extraction. *Processes*, *8*(11), 1348.

[31] Afonso, S., Silva, F. B., Silva, A. F., Scarminio, I. S., and Bruns, R. E. (2017). Infrared spectral evidence and DFT calculations of hydrogen-bonding and molecular structures of acetogenins. *Journal of Molecular Structure*, *1130*, 174–180.

[32] Le, Q., Yin, Z., Wu, J., Gao, S., Li, W., and Liao, Q. (2025). Numerical study on cavitation bubble dynamics with dual-frequency excitation in magnesium alloy melt. *Physics Letters A*, *539*, 130366.

[33] Liu, C., Hu, J., Xie, Y., Liu, Y., and Lei, W. (2023). Bubble dynamics and cavitation damage to curved elastic boundaries. *Journal of Physics: Conference Series*, *2023,* 012002.

[34] Singhania, N., Barmanray, A., and Chhikara, N. (2022). Optimization of solvent extraction conditions of bioactive compound from wood apple (*Limonia acidissima* L.) fruit using ultrasonic assisted extraction. *Journal of Food Processing and Preservation*, *46*(12), e17269.

[35] Yeasmen, N., and Orsat, V. (2024). Maximization of the recovery of phenolic compounds from sugar maple leaves. *Biomass Conversion and Biorefinery*, *14*(5), 6251–6266.

[36] Fikry, M., Jafari, S., Shiekh, K. A., Kijpatanasilp, I., Khongtongsang, S., Khojah, E., Aljumayi, H., and Assatarakul, K. (2024). Ultrasound-assisted extraction of bioactive compounds from longan seeds powder: Kinetic modelling and process optimization. *Ultrasonics Sonochemistry*, *108*, 106949.

[37] Turker, I., and Isleroglu, H. (2021). Optimization of extraction conditions of bioactive compounds by ultrasonic-assisted extraction from artichoke wastes. *Acta Chimica Slovenica*, *68*(3), 658–666.

[38] Jiskani, A. H., Aydar, A. Y., and Ahmed, D. (2021). Optimization of ultrasound-assisted extraction of antioxidant compounds from *Rumex hastatus* with response surface methodology. *Journal of Food Processing and Preservation*, *45*(11), e15983.

[39] Zorić, Z., Pedisić, S., Brnčić, M., Matanović, A., Marjanović, I., and Ninčević Grassino, A. (2025). Ultrasound-assisted extraction of polyphenols from *Laurus nobilis* leaves: Effects of process parameters. *Applied Sciences*, *15*(17), 9347.

[40] Vijayalakshmi, M., Kunjiappan, S., Ravindranath, A., Kannan, S., Sundar, K., and Pandian, S. R. K. (2025). A hybrid of RSM, ANFIS, and machine learning algorithm approach for ultrasound-assisted extraction of bioactive compounds from *Semecarpus anacardium* Linn. *Separation Science and Technology*, *60*(1), 75–93.

[41] Pradal, D., Vauchel, P., Decossin, S., Dhulster, P., and Dimitrov, K. (2016). Kinetics of ultrasound-assisted extraction of antioxidant polyphenols from food by-products: Extraction and energy consumption optimization. *Ultrasonics Sonochemistry*, *32*, 137–146.

[42] Vo, T. P., Phan, T. H., Doan Luu, N. T., Tran, T. B. X., Pham, N. Q., Ho, T. A. T., Ha, N. M. H., Nguyen, M. T., and Nguyen, D. Q. (2024). Optimization of ultrasonic-assisted extraction of phenolics and terpenoids from sweet basil leaves using natural deep eutectic solvents. *International Journal of Chemical Engineering*, *2024*(1), 5199884.

[43] Elias, H. S., Baharum, S. N., Azizan, K. A., Wan Ahmad, W. Y., Chandren, S., and Basar, N.

DOI: https://doi.org/10.17509/ijost.v11i1.94654
p- ISSN 2528-1410 e- ISSN 2527-8045

(2023). Optimization of ultrasound-assisted extraction for antioxidant activity in relation to rhoifolin content of *Fortunella polyandra* using response surface methodology (RSM). *Sains Malaysiana*, *52*(1), 153–164.

[44] Ozdemir, M., Gungor, V., Melikoglu, M., and Aydiner, C. (2024). Solvent selection and effect of extraction conditions on ultrasound-assisted extraction of phenolic compounds from galangal (*Alpinia officinarum*). *Journal of Applied Research on Medicinal and Aromatic Plants*, *38*, 100525.

[45] Ciric, A., Krajnc, B., Heath, D., and Ogrinc, N. (2020). Response surface methodology and artificial neural network approach for the optimization of ultrasound-assisted extraction of polyphenols from garlic. *Food and Chemical Toxicology*, *135*, 110976.

[46] Deng, J., Tang, N., Xu, L., Chen, F., Zhou, X., Tang, W., and Tang, X. (2025). Ultrasound extraction, quantification, and antioxidant activity of flavonoids from *Aquilaria sinensis* leaves. *Journal of Applied Research on Medicinal and Aromatic Plants*, *49*, 100664.

[47] Zapata, J. E., Sepúlveda, C. T., and Álvarez, A. C. (2022). Kinetics of the thermal degradation of phenolic compounds from achiote leaves (*Bixa orellana* L.) and its effect on the antioxidant activity. *Food Science and Technology*, *42*, e30920.

[48] Niari, S., Hamdami, N., Dalvi-Isfahan, M., and Le-Bail, A. (2025). Ultrasound and microwave assisted extraction of acorn oil (*Quercus brantii*): Optimization and characterization. *Applied Food Research*, *5*(1), 100706.

[49] Sambou, M., Jean-François, J., Ndongou Moutombi, F. J., Doiron, J. A., Hébert, M. P. A., Joy, A. P., Mai-Thi, N.-N., Barnett, D. A., Surette, M. E., Boudreau, L. H., and Touaibia, M. (2020). Extraction, antioxidant capacity, 5-lipoxygenase inhibition, and phytochemical composition of propolis from Eastern Canada. *Molecules*, *25*(10), 2397.

[50] Campos, T. A. F., Alves, E. S., Silva, N. M., Feihrmann, A. C., Cardozo-Filho, L., and Santos Junior, O. O. (2025). Bioactive compounds from black mulberry (*Morus nigra* L.) leaves: Optimization of ultrasonic extraction and encapsulation with sodium alginate. *LWT*, *232*, 118469.

[51] Mahindrakar, K. V., and Rathod, V. K. (2022). Ultrasound-assisted intensified aqueous extraction of phenolics from waste *Syzygium cumini* leaves: Kinetic studies and evaluation of antioxidant, antidiabetic and anticancer potential. *Food Bioscience*, *46*, 101547.

[52] Rathod, V. K., G, K., and Gharat, N. N. (2022). Kinetics of extraction of total phenolic content from *Sesbania grandiflora* L. leaves using ultrasound. *Indian Chemical Engineer*, *64*(3), 266–276.

[53] Sukor, N. F., Jusoh, R., Kamarudin, N. S., Abdul Halim, N. A., Sulaiman, A. Z., and Abdullah, S. B. (2020). Synergistic effect of probe sonication and ionic liquid for extraction of phenolic acids from oak galls. *Ultrasonics Sonochemistry*, *62*, 104876.

[54] Riguene, H., Dali, S., Salem, R. B., and Rigane, G. (2022). Optimization of ultrasound-assisted extraction of phenolic compounds from *Verbena officinalis* L. leaves using response surface methodology and evaluation of its antioxidant activities. *Revue Roumaine de Chimie*, *67*(6–7), 393–406.

[55] Soufi, O., Medouni-Haroune, L., Bachirbey, M., Medouni-Adrar, S., Idir, F., Heddad, T., Ouldsaadi, L., Romero, C., Madani, K., and Makhlouf-Boulekbache, L. (2023). Statistical optimization of ultrasound-assisted extraction of polyphenols from olive pomace. *Sustainable Chemistry and Pharmacy*, *36*, 101260.

[56] Rizkita, N., Machmudah, S., Wahyudiono, Winardi, S., Adschiri, T., and Goto, M. (2023). Phytochemical compounds extraction from *Orthosiphon aristatus*, *Andrographis paniculata*, *Gynura segetum* using hydrothermal method: Experimental kinetics and

DOI: https://doi.org/10.17509/ijost.v11i1.94654
p- ISSN 2528-1410 e- ISSN 2527-8045

modeling. *South African Journal of Chemical Engineering*, *46*, 330–342.

[57] Martín-García, B., Montijo-Prieto, S. D., Jiménez-Valera, M., Carrasco-Pancorbo, A., Ruiz-Bravo, A., Verardo, V., and Gómez-Caravaca, A. M. (2022). Comparative extraction of phenolic compounds from olive leaves using a sonotrode and an ultrasonic bath and the evaluation of both antioxidant and antimicrobial activity. *Antioxidants*, *11*(3), 558.

[58] Ilgaz, C., Kelebek, H., and Kadiroglu, P. (2024). Bioactivity, DNA damage protecting, and aroma potential of oleuropein enriched olive leaf extract by optimization of ultrasound-assisted process. *eFood*, *5*(1), e134.

[59] Dukić, J., Režek Jambrak, A., Jurec, J., Merunka, D., Valić, S., Radičić, R., Krstulović, N., Nutrizio, M., and Dubrović, I. (2025). High-power ultrasound and high-voltage electrical discharge-assisted extractions of bioactive compounds from sugar beet (*Beta vulgaris* L.) waste: Electron spin resonance and optical emission spectroscopy analysis. *Molecules*, *30*(4), 796.

[60] Shekhar, S., Prakash, P., Singha, P., Prasad, K., and Singh, S. (2023). Modeling and optimization of ultrasound-assisted extraction of bioactive compounds from *Allium sativum* leaves using response surface methodology and artificial neural network coupled with genetic algorithm. *Foods*, *12*(9), 1925.

[61] Ebrahimi, P., Bayram, I., Mihaylova, D., and Lante, A. (2025). A strategy to minimize the chlorophyll content in the phenolic extract of sugar beet leaves: Can this extract work as a natural antioxidant in vegetable oils? *Food and Bioprocess Technology*, *18*(3), 2493–2506.

[62] Gavamukulya, Y., Abou-Elella, F., Wamunyokoli, F., and El-Shemy, H. A. (2015). GC-MS analysis of bioactive phytochemicals present in ethanolic extracts of leaves of *Annona muricata*: A further evidence for its medicinal diversity. *Pharmacognosy Journal*, *7*(5), 300–304.

[63] Shibula, K., and Velavan, S. (2015). Determination of phytocomponents in methanolic extract of *Annona muricata* leaf using GC-MS technique. *International Journal of Pharmacognosy and Phytochemical Research*, *7*(6), 1251–1255.

[64] Pant, P., Khulbe, K., and Pant, C. C. (2024). Phytochemical constituents, antioxidant, and antibacterial activities of Himalayan *Indigofera dosua* leaf extract. *Journal of Herbs, Spices and Medicinal Plants*, *30*(4), 456–468.

[65] Gözcü, S., Akşit, Z., Aydın, A., Yılmaz, M. A., and Şimşek, S. (2025). Comprehensive phenolic profiling and biological evaluation of *Centaurea glastifolia* L. (Asteraceae). *Natural Product Research*, *39*(4), 633–644.

[66] Abdallah, R. H., Al-Attar, A. R., Shehata, Y. M., Abdel-Fattah, D. M., Atta, R. M., Fantoukh, O. I., and Mustafa, A. M. (2024). Comprehensive chemical profiling and mechanistic insight into anticancer activity of *Annona muricata* leaves extract. *Pharmaceuticals*, *17*(5), 614.

[67] Oufquir, S., Agouram, F., Kabdy, H., Laaradia, M. A., Oubella, K., Abdelmoniim, B., Rachida, A., Garzoli, S., and Chait, A. (2025). Novel insights into the bioactive profile and therapeutic potentials of Indonesian *Annona muricata* leaves. *Chemistry & Biodiversity*, , *2025*, e01606.

[68] Nee, C. A., Noorhadi, N. H., Sofian-Seng, N.-S., Mediani, A., Lim, S. J., and Rahman, H. A. (2024). Phytochemical content, antioxidant, antihyperglycemic, and antiobesityactivities of *Annona muricata* leaf extract with different polarities. *Sains Malaysiana*, *53*(8), 1913–1924.

[69] Nguyen, M. T., Nguyen, V. T., Minh, L. V., Ly, H. T., Cang, M. H., Bui, L. B., Le, X. T., and Danh, V. T. (2020). Determination of the phytochemical screening, total polyphenols,

DOI: https://doi.org/10.17509/ijost.v11i1.94654
p- ISSN 2528-1410 e- ISSN 2527-8045

flavonoids content, and antioxidant activity of soursop leaves (*Annona muricata* Linn.). *IOP Conference Series Materials Science and Engineering*, *736*(6), 062011.

[70] Safarzaei, A. S., Esmaeilzadeh Kenari, R., and Farahmandfar, R. (2023). Optimization of aqueous extraction conditions of phenolic and antioxidant compounds of Caper (*Capparis spinosa*) leaves and roots using response surface. *Journal of Food Science and Technology*, *20*(138), 26–40.

DOI: https://doi.org/10.17509/ijost.v11i1.94654
p- ISSN 2528-1410 e- ISSN 2527-8045

Table 7. Kinetics of soursop leaf powder extraction for yield.

Model	R^2	RMSE	AIC	BIC	Equation Parameters						
					1	2	3	4	5	6	7
Yield, 70:30, 10%											
Poly 5	1.000	2.962E-15	-389.433	-390.683	p_1 = -2.250	p_2 = 0.689	p_3 = 5.230	p_4 = -1.787	p_5 = -2.364	p_6 = 3.719	-
Gaussian Mixture 2	0.912	0.153	-8.528	-9.985	p_1 = 1.443	p_2 = 437.025	p_3 = 56.350	p_4 = 0.755	p_5 = 666.311	p_6 = 49.775	p_7 = 2.725
Ex-Gaussian	0.901	0.162	-11.829	-12.870	A = 246.638	μ = 400.846	σ = 45.402	τ = 80.192	b = 2.766	-	-
Yield, 70:30, 50%											
Poly 4	0.908	0.174	-10.977	-12.018	p_1 = -1.115	p_2 = 0.676	p_3 = 1.812	p_4 = -1.082	p_5 = 2.931		-
Poly 5	1.000	1.944E-15	-394.487	-395.736	p_1 = -1.293	p_2 = -1.115	p_3 = 3.652	p_4 = 1.812	p_5 = -2.293	p_6 = 2.931	-
Yield, 70:30, 90%											
Poly 4	0.951	0.140	-13.558	-14.599	p_1 = 1.041	p_2 = 0.124	p_3 = -2.240	p_4 = -0.732	p_5 = 3.625	-	-
Poly 5	1.000	1.439E-15	-398.098	-399.347	p_1 = -1.043	p_2 = 1.041	p_3 = 2.524	p_4 = -2.240	p_5 = -1.709	p_6 = 3.625	-
Yield, 85:15, 10%											
Poly 4	0.918	7.561E-02	-20.986	-22.027	p_1 = 0.766	p_2 = 0.160	p_3 = -1.501	p_4 = -0.298	p_5 = 2.383	-	-
Poly 5	1.000	1.164E-15	-400.639	-401.888	p_1 = 0.561	p_2 = 0.766	p_3 = -1.132	p_4 = -1.501	p_5 = 0.228	p_6 = 2.383	-
Yield, 85:15, 50%											
Cubic	0.960	7.309E-02	-23.393	-24.226	p_1 = 2.966E-08	p_2 = -4.745E-05	p_3 = 2.246E-02	p_4 = -1.093	-	-	-
Poly 4	0.975	5.838E-02	-24.090	-25.131	p_1 = 0.145	p_2 = 0.655	p_3 = -0.340	p_4 = -0.795	p_5 = 1.974	-	-
Poly 5	1.000	4.347E-16	-412.461	-413.711	p_1 = 0.434	p_2 = 0.145	p_3 = -0.342	p_4 = -0.340	p_5 = -0.389	p_6 = 1.974	-
Yield, 85:15, 90%											
Poly 5	1.000	1.013E-15	-402.305	-403.554	p_1 = -1.043	p_2 =-0.276	p_3 = 2.382	p_4 = 0.179	p_5 = -1.044	p_6 = 2.334	-
Yield, 100:0, 10%											
Cubic	0.936	8.419E-02	-21.696	-22.529	p_1 = -2.403E-08	p_2 = 3.539E-05	p_3 = -1.500E-02	p_4 = 3.900	-	-	-
Poly 4	0.948	7.561E-02	-20.986	-22.027	p_1 = -0.122	p_2 = -0.531	p_3 = 4.375E-02	p_4 = 0.643	p_5 = 2.253	-	-
Poly 5	1.000	3.392E-16	-415.440	-416.689	p_1 = -0.561	p_2 = -0.123	p_3 = 0.761	p_4 = 4.375E-02	p_5 = 0.117	p_6 = 2.253	-
Yield, 100:0, 50%											
Cubic	0.984	5.891E-02	-25.981	-26.814	p_1 = -1.726E-08	p_2 = 1.965E-05	p_3 = -4.636E-03	p_4 = 1.887	-	-	-
Poly 4	0.999	1.106E-02	-44.055	-45.096	p_1 = -0.191	p_2 = -0.381	p_3 = -0.222	p_4 = 0.484	p_5 = 2.292	-	-
Poly 5	1.000	4.622E-16	-411.726	-412.975	p_1 = -0.082	p_2 = -0.191	p_3 = -0.192	p_4 = -0.222	p_5 = 0.407	p_6 = 2.292	-
Asymmetric Gaussian	1.000	1.301E-03	-69.738	-70.779	A = 1.542	μ =710.032	σ_L = 431.539	σ_R =85.896	b = 0.886	-	-
Yield, 100:0, 90%											
Poly 5	1.000	3.951E-15	-385.978	-387.228	p_1 = -2.912	p_2 = -0.094	p_3 = 6.871	p_4 = 0.671	p_5 = -2.777	p_6 = 1.008	-

DOI: https://doi.org/10.17509/ijost.v11i1.94654
p- ISSN 2528-1410 e- ISSN 2527-8045

Table 8. Kinetics of soursop leaf powder extraction for yield × TPC.

Model	R^2	RMSE	AIC	BIC	Equation Parameters					
					1	2	3	4	5	6
Yield × TPC, 70:30, 10%										
Cubic	0.960	0.322	-5.608	-6.441	p_1 = -1.043E-07	p_2 = 1.472E-04	p_3 = -5.464E-02	p_4 = 22.610	-	-
Poly 4	0.965	0.302	-4.381	-5.423	p_1 = 0.370	p_2 = -2.304	p_3 = -2.058	p_4 = 3.848	p_5 = 19.565	-
Poly 5	1.000	6.15E-15	-380.661	-381.911	p_1 = 2.240	p_2 = 0.370	p_3 = -7.461	p_4 = -2.058	p_5 = 5.947	p_6 = 19.565
Gaussian Peak	0.962	0.311	-5.997	-6.830	A = 4.524	μ = 650.201	σ = 108.914	b = 16.923	-	-
Asymmetric Gaussian	0.980	0.227	-7.815	-8.856	A = 5.115	μ = 698.734	σ_L = 136.172	σ_R = 51.387	b = 16.948	-
Ex-Gaussian	0.962	0.312	-3.996	-5.037	A = 1237.010	μ = 646.784	σ = 109.165	τ = 3.294	b = 16.922	-
Yield × TPC, 70:30, 50%										
Poly 4	0.994	0.201	-9.232	-10.273	p_1 = -4.265	p_2 = 3.650	p_3 = 6.564	p_4 = -6.039	p_5 = 18.168	-
Poly 5	1.000	7.288E-15	-378.630	-379.880	p_1 = -1.495	p_2 = -4.265	p_3 = 7.092	p_4 = 6.564	p_5 = -7.440	p_6 = 18.168
Yield × TPC, 70:30, 90%										
Poly 5	1.000	6.024E-15	-380.916	-382.166	p_1 = -4.673	p_2 = 4.367	p_3 = 10.257	p_4 = -9.682	p_5 = -5.947	p_6 = 20.909
Yield × TPC, 85:15, 10%										
Poly 4	0.942	0.480	1.202	0.161	p_1 = 6.043	p_2 = 1.287	p_3 = -11.920	p_4 = -1.855	p_5 = 19.481	-
Poly 5	1.000	4.166E-15	-385.342	-386.591	p_1 = 3.568	p_2 = 6.043	p_3 = -6.924	p_4 = -11.920	p_5 = 1.487	p_6 = 19.481
Yield × TPC, 85:15, 50%										
Poly 5	1.000	6.725E-15	-379.595	-380.844	p_1 = 5.296	p_2 = 2.402	p_3 = -7.210	p_4 = -5.460	p_5 = -1.551	p_6 = 17.103
Yield × TPC, 85:15, 90%										
Poly 5	1.000	8.702E-05	-376.502	-377.752	p_1 = -5.137	p_2 = -1.312	p_3 = 12.869	p_4 = -0.174	p_5 = -6.094	p_6 = 18.899
Yield × TPC, 100:0, 10%										
Cubic	0.952	0.243	-9.000	-9.833	p_1 =-7.745E-08	p_2 = 1.111E-04	p_3 = -0.045	p_4 = 16.450	-	-
Poly 4	0.953	0.241	-7.051	-8.093	p_1 = 0.074	p_2 = -1.712	p_3 = -0.998	p_4 = 2.190	p_5 = 12.361	-
Poly 5	1.000	1.256E-15	-399.729	-400.979	p_1 = -1.793	p_2 = 0.074	p_3 = 2.416	p_4 = -0.998	p_5 = 0.510	p_6 = 12.361
Yield × TPC, 100:0, 50%										
Cubic	0.976	0.380	-3.619	-4.452	p_1 = -9.962E-08	p_2 = 1.188E-04	p_3 = -0.032	p_4 = 11.173	-	-
Poly 4	0.994	0.194	-9.669	-10.710	p_1 = -1.080	p_2 = -2.201	p_3 = -0.909	p_4 = 2.887	p_5 = 12.220	-
Poly 5	1.000	2.640E-15	-390.817	-392.067	p_1 = -1.442	p_2 = -1.080	p_3 = 1.117	p_4 = -0.909	p_5 = 1.536	p_6 = 12.220
Asymmetric Gaussian	0.998	0.106	-16.922	-17.963	A = 7.325	μ = 729.623	σ_L = 421.898	σ_R = 55.812	b = 5.665	-
Yield × TPC, 100:0, 90%										
Poly 5	1.000	1.631E-14	-368.962	-370.211	p_1 = -16.203	p_2 = -2.210	p_3 = 39.162	p_4 = 6.129	p_5 = -16.465	p_6 = 7.429

DOI: https://doi.org/10.17509/ijost.v11i1.94654
p- ISSN 2528-1410 e- ISSN 2527-8045

Table 9. Kinetics of soursop leaf powder extraction for yield × TFC.

Model	R^2	RMSE	AIC	BIC	Equation Parameters					
					1	2	3	4	5	6
Yield × TFC, 70:30, 10%										
Cubic	0.937	2.453E-02	-36.493	-37.326	p_1 = -5.862E-09	p_2 = 9.235E-06	p_3 = -3.924E-03	p_4 = 1.115	-	-
Poly 4	0.949	2.199E-02	-35.807	-36.848	p_1 = -3.598E-02	p_2 = -0.129	p_3 = 7.120E-02	p_4 = 0.262	p_5 = 0.739	-
Poly 5	1.000	3.006E-16	-416.887	-418.136	p_1 = 0.163	p_2 = -3.598E-02	p_3 = -0.505	p_4 = 7.120E-02	p_5 = 0.415	p_6 = 0.739
Asymmetric Gaussian	0.953	2.117E-02	-36.263	-37.304	A = 0.267	μ = 629.364	σ_L = 33.359	σ_R = 228.335	b = 0.664	-
Ex-Gaussian	0.953	2.117E-02	-36.263	-37.304	A = 107.725	μ = 601.002	σ = 27.433	τ = 266.494	b = 0.664	-
Yield × TFC, 70:30, 50%										
Poly 4	0.956	1.540E-02	-40.077	-41.118	p_1 = -0.190	p_2 = 7.051E-02	p_3 = 0.338	p_4 = -9.196E-02	p_5 = 0.713	-
Poly 5	1.000	5.286E-16	-410.116	-411.366	p_1 = -0.114	p_2 = -0.190	p_3 = 0.334	p_4 = 0.338	p_5 = -0.199	p_6 = 0.713
Yield × TFC, 70:30, 90%										
Poly 5	1.000	4.003E-16	-413.452	-414.701	p_1 = -0.267	p_2 = 6.151E-02	p_3 = 0.556	p_4 = -0.129	p_5 = -0.182	p_6 = 0.813
Yield × TPC, 85:15, 10%										
Cubic	0.953	1.840E-02	-39.943	-40.776	p_1 = -2.738E-09	p_2 = 4.385E-06	p_3 = -1.728E-03	p_4 = 1.039	-	-
Poly 4	0.982	1.152E-02	-43.563	-44.604	p_1 = -4.747E-02	p_2 = -6.051E-02	p_3 = 9.778E-02	p_4 = 0.172	p_5 = 0.924	-
Poly 5	1.000	3.392E-16	-415.440	-416.689	p_1 = -8.556E-02	p_2 = -4.747E-02	p_3 = 0.136	p_4 = 9.778E-02	p_5 = 9.172E-02	p_6 = 0.924
Gaussian Peak	0.983	1.105E-02	-46.066	-46.899	A = 0.221	μ = 787.842	σ = 153.792	b = 0.864	-	-
Asymmetric Gaussian	0.990	8.476E-03	-47.246	-48.287	A = 0.281	μ = 895.695	σ_L = 212.647	σ_R = 4.351	b = 0.859	-
Ex-Gaussian	0.983	1.106E-02	-44.055	-45.097	A = 85.283	μ = 780.846	σ = 154.468	τ = 6.624	b = 0.864	-
Yield × TFC, 85:15, 50%										
Cubic	0.924	2.636E-02	-35.633	-36.466	p_1 =1.660-E-09	p_2 = -3.599E-06	p_3 = 2.495E-03	p_4 = 5.003E-01	-	-
Poly 4	0.986	1.124E-02	-43.861	-44.902	p_1 = 7.886E-02	p_2 = 3.668E-02	p_3 = -0.230	p_4 = 2.485E-02	p_5 = 1.091	-
Poly 5	1.000	2.027E-16	-421.618	-422.867	p_1 = -8.346E-02	p_2 = 7.886E-02	p_3 = 0.229	p_4 = -0.230	p_5 = -5.333E-02	p_6 = 1.091
Asymmetric Gaussian	0.973	1.556E-02	-39.959	-41.000	A = 0.266	μ = 415.379	σ_L = 90.181	σ_R = 750.000	b = 0.810	-
Gamma Peak	0.915	2.778E-02	-35.002	-35.834	p_1 = 3.005E-05	p_2 = 2.741	p_3 = 357.903	p_4 = 0.687	-	-
Ex-Gaussian	0.936	2.412E-02	-34.696	-35.737	A = 277.087	μ = 350.341	σ = 98.227	τ = 750.000	b = 0.821	-

DOI: https://doi.org/10.17509/ijost.v11i1.94654
p- ISSN 2528-1410 e- ISSN 2527-8045

Model	R^2	RMSE	AIC	BIC	Equation Parameters					
					1	2	3	4	5	6
Yield × TFC, 85:15, 90%										
Cubic	0.975	2.332E-02	-37.100	-37.933	p_1 = 4.074E-09	p_2 = -8.068E-06	p_3 = 5.040E-03	p_4 = 9.400E-02	-	-
Poly 4	0.985	1.782E-02	-38.328	-39.369	p_1 = -4.977E-02	p_2 = 9.003E-02	p_3 = -3.358E-02	p_4 = -1.766E-02	p_5 = 1.085	-
Poly 5	1.000	3.765E-16	-414.188	-415.437	p_1 = -0.132	p_2 = -4.977E-02	p_3 = 0.395	p_4 = -3.358E-02	p_5 = -0.142	p_6 = 1.085
Weibull	0.975	2.318E-02	-39.175	-39.799	C_∞ = 1.077	α = 151.162	β =1.484	-	-	-
Asymmetric Gaussian	0.969	2.605E-02	-33.771	-34.813	A = 0.445	μ = 366.252	σ_L = 80.625	σ_R = 750.000	b = 0.676	-
Gamma Peak	0.963	2.844E-02	-34.720	-35.553	p_1 = 1.108	p_2 = 1.209	p_3 = 2830.227	p_4 = -2.313	-	-
Yield × TFC, 100:0, 10%										
Poly 5	1.000	2.027E-16	-421.618	-422.867	p_1 = -0.165	p_2 = 6.865E-02	p_3 = 0.383	p_4 = -0.178	p_5 = -0.169	p_6 = 0.875
Gaussian Peak	0.941	1.095E-02	-46.175	-47.008	A = 0.230	μ = 507.852	σ = 49.841	b = 0.783	-	-
Asymmetric Gaussian	0.953	9.708E-03	-45.618	-46.659	A = 0.157	μ = 316.764	σ_L = 5.843	σ_R = 183.669	b = 0.779	-
Ex-Gaussian	0.950	9.994E-03	-45.270	-46.311	A = 26.275	μ = 415.857	σ = 51.727	p_4 = 95.967	b = 0.779	-
Yield × TFC, 100:0, 50%										
Cubic	0.969	1.117E-02	-45.938	-46.771	p_1 = -2.697E-09	p_2 = 3.636E-06	p_3 = -1.117E-03	p_4 = 0.731	-	-
Poly 5	1.000	1.869E-16	-422.593	-423.842	p_1 = 5.939E-02	p_2 = -2.578E-02	p_3 = -0.196	p_4 = 1.786E-03	p_5 = 0.188	p_6 = 0.746
Poly 4	0.984	7.998E-03	-47.943	-48.984	p_1 = -2.578E-02	p_2 = -5.960E-02	p_3 = 1.786E-03	p_4 = 0.132	p_5 = 0.746	-
Gaussian Peak	0.981	8.660E-03	-48.989	-49.822	A = 0.175	μ = 680.054	σ = 156.030	b = 0.642	-	-
Asymmetric Gaussian	0.987	7.198E-03	-49.207	-50.248	A = 0.179	μ = 707.187	σ_L = 190.388	σ_R = 136.680	b = 0.636	-
Ex-Gaussian	0.981	8.688E-03	-46.950	-47.991	A = 69.524	μ = 671.008	σ = 158.119	τ = 8.700	b = 0.641	-
Yield × TFC, 100:0, 90%										
Poly 5	1.000	4.924E-16	-410.968	-412.217	p_1 = -0.445	p_2 = -6.380E-03	p_3 = 1.142	p_4 = 3.168E-02	p_5 = -0.485	p_6 = 0.861

DOI: https://doi.org/10.17509/ijost.v11i1.94654
p- ISSN 2528-1410 e- ISSN 2527-8045

Table 10. ANOVA and effect size for antioxidant activity, phytochemicals, and color.

Analysis	Source	DF	Adj SS	Adj MS	F-value	p-value	η^2	ε^2
IC_{50}	Sample	7	103067	14723.8	23293.07	< 0.0001	1.000	1.000
	Error	13	8	0.6				
	Total	20	103075					
Total tannins	Sample	7	12579332	1797047	164718.97	< 0.0001	1.000	1.000
	Error	13	142	11				
	Total	20	12579474					
Total alkaloids	Sample	7	22716.2	3245.17	4132.55	< 0.0001	1.000	0.999
	Error	13	10.2	0.79				
	Total	20	22726.4					
Total saponins	Sample	7	27.7405	3.96293	1958.16	< 0.0001	0.999	0.998
	Error	13	0.0263	0.00202				
	Total	20	27.7668					
Total steroids	Sample	7	2993187	427598	14440.85	< 0.0001	1.000	1.000
	Error	13	385	30				
	Total	20	2993572					
Color - L	Sample	7	9105.09	1300.73	6503636.23	< 0.0001	1.000	1.000
	Error	13	0	0				
	Total	20	9105.09					
Color – a*	Sample	7	81.847	11.6924	87693.17	< 0.0001	1.000	1.000
	Error	13	0.0017	0.0001				
	Total	20	81.8487					
Color – b*	Sample	7	1292.91	184.702	1565950.76	< 0.0001	1.000	1.000
	Error	13	0	0				
	Total	20	1292.91					

Note: All effects significant at $p < 0.001$ (Tukey's test); partial $\eta^2 = 1.0$ and $\varepsilon^2 = 1$ indicate very large effects

DOI: https://doi.org/10.17509/ijost.v11i1.94654
p- ISSN 2528-1410 e- ISSN 2527-8045

Table 11. Effect size (Cohen's d) dan SD_{pooled} between treatments.

Sample	IC_{50}		Total tannins		Total alkaloids		Total saponins	
	SD_{pooled}	d, Cohen	SD_{pooled}	d, Cohen	SD_{pooled}	d, Cohen	SD_{pooled}	d, Cohen
UAE 100:0, 10%, 7.5 min	1.007	67.817	3.464	506.646	0.037	205.733	0.024	78.592
UAE 85:15, 90%, 5 min	0.551	138.937	3.514	514.247	0.069	272.454	0.026	75.710
UAE 70:30, 50%, 10 min	0.469	190.792	4.348	481.800	1.306	74.287	0.030	86.527
Soxhlet 70:30, 2× cycle time	0.621	261.656	4.387	551.023	0.302	146.628	0.024	112.075
Commercial product 1	0.688	311.564	3.501	701.085	0.685	100.701	0.022	179.354
Commercial product 2	0.646	284.201	3.488	583.049	0.529	113.549	0.074	43.156
	Total steroids		**Color – L**		**Color – a***		**Color – b***	
UAE 100:0, 10%, 7.5 min	4.347	242.049	1.826E-02	2252.600	1.732E-02	239.600	1.155E-02	1438.468
UAE 85:15, 90%, 5 min	7.168	142.666	1.826E-02	2083.902	1.472E-02	212.415	1.155E-02	1328.483
UAE 70:30, 50%, 10 min	4.384	249.578	1.826E-02	2014.341	1.472E-02	189.317	1.472E-02	1064.340
Soxhlet 70:30, 2× cycle time	4.423	259.517	2.041E-02	1952.897	1.291E-02	173.251	9.129E-03	1819.899
Commercial product 1	4.465	251.147	2.041E-02	506.391	1.472E-02	418.263	9.129E-03	163.586
Commercial product 2	4.423	214.906	2.041E-02	163.299	1.472E-02	23.551	1.155E-02	58.890

Note: Effect sizes (Cohen's d) were calculated for raw materials (fresh) using pooled SD for each metric.

Table 12. Chemical composition per class (% relative area) in each sample.

No	Chemical Categories	Area Relatif (%)						
		Fresh	R100	R85	R70	Soxhlet	P1	P2
1	Heterocyclic N–S/N–O (nitrogen base)	11.28	7.96	17.09	0	0	0	0
2	Phenolics and derivatives	18.93	9.54	22.17	2.45	0	28.55	8.83
3	Phenolic organic acids (quinic acid)	18.08	0	15.35	2.64	0	4.44	0
4	Carbohydrates and derivatives (including polyols)	8.18	6.98	2.85	94.91	100.00	3.29	0
5	Terpenoids (hydrocarbons and alcohols)	19.85	41.33	19.56	0	0	28.30	5.12
6	Saturated/unsaturated fatty acids and their esters	23.68	34.19	9.47	0	0	35.42	86.04
7	Other esters (glycerol/oxirane)	0	0	10.44	0	0	0	0
8	Secondary aliphatic amines	0	0	3.09	0	0	0	0
	Total identified (≈% TIC)	79.91	81.37	86.21	92.74	98.11	87.82	79.82

Note: TIC = total ion chromatogram.

DOI: https://doi.org/10.17509/ijost.v11i1.94654
p- ISSN 2528-1410 e- ISSN 2527-8045